

Review

Rechargeable anion-shuttle batteries for low-cost energy storage

Qi Liu,^{1,2,5} Yizhou Wang,^{3,5} Xu Yang,³ Dong Zhou,^{3,*} Xianshu Wang,¹ Pauline Jaumaux,³ Feiyu Kang,¹ Baohua Li,^{1,*} Xiulei Ji,^{4,*} and Guoxiu Wang^{3,*}

SUMMARY

As promising alternatives to lithium-ion batteries, rechargeable anion-shuttle batteries (ASBs) with anions as charge carriers stand out because of their low cost, long cyclic lifetime, and/or high energy density. In this review, we provide for the first time, comprehensive insights into the anion shuttling mechanisms of ASBs, including anion-based rocking-chair batteries (ARBs), dual-ion batteries (DIBs), including insertion-type, conversion-type, and conversion-insertion-type, and reverse dual-ion batteries (RDIBs). Thereafter, we review the latest progresses and challenges regarding electrode materials and electrolytes for ASBs. In addition, we summarize the existing dilemmas of ASBs and outline the perspective of ASB technology for future grid storage.

INTRODUCTION

Stationary energy storage technology is considered as a key technology for future society, especially to support the ecological transition toward renewable energies.¹ Among the available technologies (e.g., rechargeable batteries, fly wheels, and compressed air energy storage), rechargeable batteries are the most promising candidates for stationary energy storage because of their fast response, flexible configuration, and relatively easier construction.² Lithium (Li)-ion batteries have revolutionized energy storage technology since their introduction in portable electronic devices in 1991.³ In the past few decades, they have quickly dominated the markets of portable electronic and electric vehicle because of their high gravimetric and volumetric energy density.⁴ However, they are economically uncompetitive for stationary energy storage because of the limited resources of Li and transition metals in the earth's crust. Thus, there is an urgent need to develop suitable battery systems for stationary energy storage. In recent years, metal-ion batteries with low-cost metal ions as charge carriers, including alkali metal-ion batteries (e.g., sodium (Na)-ion and potassium (K)-ion batteries) and multivalent metal-ion-batteries (e.g., calcium (Ca)-ion, magnesium (Mg)-ion, aluminum (Al)-ion, and zinc (Zn)-ion batteries), have demonstrated their capability to be viable alternatives to Li-ion batteries for large-scale applications.⁵ However, great efforts are still needed to tackle their limited energy density and lifetime cost.

More recently, rechargeable anion-shuttle batteries (ASBs) have emerged as a novel battery concept and attracted significant interest from the research community. As their name implies, the mechanism of ASBs is based on anions (e.g., HSO_4^- ,⁶ ClO_4^- ,⁷ PF_6^- ,⁸ F^- ,⁹ and Cl^- ,¹⁰) as charge carriers, shuttling between electrodes through the electrolyte. Unlike metal ions, which form ionic bonds with host materials, anions generally form hybrid covalent-ionic bonds within the host materials.

The bigger picture

Lithium-ion batteries have so far remained the prevailing energy storage devices in mobile devices and electric vehicle markets. However, the relatively high cost of lithium and transition metal compounds in electrodes hinders their potential applications in grid energy storage. As an alternative energy storage strategy, rechargeable anion-shuttle batteries (ASBs) with anions, as charge carriers compensating charge neutrality of electrodes, have attracted great attention because of the prospect of low costs, long cycle life, and/or high energy density. Unraveling the anion-shuttle chemistries will benefit immensely the future development of high-performance batteries. This review presents a purview of emerging ASBs, including anion-based rocking-chair batteries (ARBs), dual-ion batteries (DIBs), including insertion-type, conversion-type, and conversion-insertion-type, and reverse dual-ion batteries (RDIBs). Their corresponding charge storage mechanisms, battery configurations, recent advances in electrode and electrolyte materials, challenges, and prospects are discussed in detail.

This unique characteristic of anions enables them not only to insert into host materials but also to perform conversion or conversion-insertion reactions within the host materials.¹¹ ASBs exhibit obvious merits over traditional alkali-metal-ion batteries, including: (1) long cycling lifetime and/or high energy/power density; (2) low manufacturing costs due to the resource abundance of non-metallic charge carriers and the wide application of inexpensive electrode materials (e.g., graphite); and (3) environmental friendliness and improved safety due to the wide use of aqueous or solid-state electrolytes. All these facilitate their applications for grid-scale energy storage.¹¹

A timeline of the development of ASBs is shown in **Figure 1**. The concept of ASBs was developed from fundamental research on flakes of crystalline graphite in a solution of sulfuric acid, where an interesting phenomenon of anion intercalation into graphite was reported.¹² However, at that time, this anion intercalation phenomenon had not been deeply studied. In 1938, Rüdorff et al. reported a reversible anion-shuttle cell with graphite as both cathode and anode, along with the concentrated sulfuric acid as the electrolyte.⁶ The reversible intercalation process of HSO_4^- into graphite is seen as the earliest ancestor of ASBs. Anion-based rocking-chair batteries (ARBs) were further developed on the basis of halogen-ion shuttling. In 2011, Reddy et al. reported a new type of ASBs, in which fluoride ions acted as the charge transfer carrier between a metal anode and a metal fluoride cathode.⁹ Subsequently, in 2013, Zhao et al. reported another type of ARB based on chloride ion shuttling.¹⁰ The cell was composed of a metal anode and a metal chloride cathode, where a binary ionic liquid was employed as the electrolyte. Contemporaneously, aqueous ARBs have also been developed.^{13,14}

In parallel with the development of halogen ion-shuttle batteries, dual-ion batteries (DIBs) emerged in 1989. McCullough et al. proposed a pioneer non-aqueous rechargeable DIB based on anion-intercalation in cathode.¹⁵ Soon after, Panero et al. designed a new type of DIB by employing graphite as anode and polypyrrole (PPy) as cathode in a carbonate-based electrolyte.⁷ They claimed that the “rocking-chair” terminology did not accurately describe this type of battery chemistry; thus, the terms “dual-ion cell” or “di-ion cell” were adopted. In the meantime, Carlin et al. reported the electrochemical characteristics of the intercalation of various anions (e.g., the aluminum-based superhalogen ion AlCl_4^- ; tetrafluoride borate ion BF_4^- ; and hexafluorophosphate ion PF_6^-) into graphite cathodes in an ionic liquid-based electrolyte.¹⁶ Furthermore, in 2000, Dahn et al. conducted an in-depth investigation by *in situ* X-ray diffraction (XRD) into intercalation of PF_6^- anions into graphite in Li metal||graphite cells. They proposed the possible practical application of DIBs in energy storage.⁸ Then, in 2012, Placke et al. developed a graphite||graphite DIB, where both cations and anions participated in electrochemical reactions during the charge-discharge processes. Other anode materials (e.g., $\text{Li}_4\text{Ti}_5\text{O}_{12}$) were also applied in DIBs.¹⁷ In 2018, Jiang et al. demonstrated DIB chemistry in an aqueous electrolyte with reversible electrochemical insertion of NO_3^- into manganese (II, III) oxide (Mn_3O_4) as cathode material.¹⁸ In 2019, Yang et al. proposed a high-energy aqueous DIB based on a reversible halogen conversion-intercalation into graphite cathodes, where anions acted as reversible redox centers for charge transfer.¹⁹ Such conversion-insertion-type DIB delivered a high energy density with good cycling stability. Based on the research into DIBs, in 2019, a new concept of “reverse dual-ion batteries (RDIBs)” was proposed, using a highly concentrated aqueous electrolyte in which anions intercalated into the anode while the cation-deficient cathode hosted cations during discharge.²⁰

¹Shenzhen Key Laboratory of Power Battery Safety and Shenzhen Geim Graphene Center, Tsinghua Shenzhen International Graduate School, Tsinghua University, Shenzhen 518055, China

²School of Materials Science and Engineering, Tsinghua University, Beijing 100084, China

³Centre for Clean Energy Technology, Faculty of Science, University of Technology Sydney, Sydney, NSW 2007, Australia

⁴Department of Chemistry, Oregon State University, Corvallis, OR 97331-4003, USA

⁵These authors contributed equally

*Correspondence:
zhoodong087@gmail.com (D.Z.),
libh@mail.sz.tsinghua.edu.cn (B.L.),
david.ji@oregonstate.edu (X.J.),
guoxiu.wang@uts.edu.au (G.W.)

<https://doi.org/10.1016/j.chempr.2021.02.004>

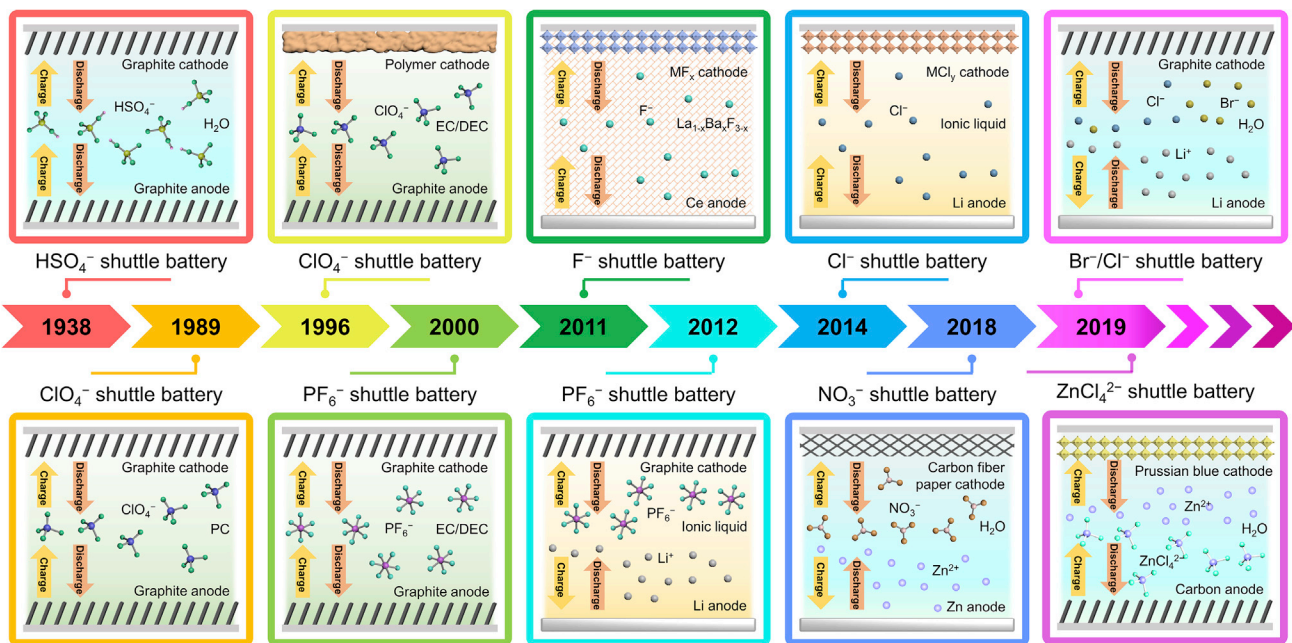


Figure 1. Timeline of the development of anion-shuttle-based batteries

PC, EC, and DEC represent propylene carbonate, ethylene carbonate, and diethyl carbonate, respectively

In recent years, ASBs have inspired research enthusiasm in both electrochemistry and material science communities. Extensive efforts have been made, focusing on in-depth understanding of the anion-shuttle mechanisms, and screening suitable electrode and electrolyte materials for ASBs. Herein, for the first time, we comprehensively outline the working mechanisms and chemical characteristics of different types of ASBs. In addition, we review the recent advances in the developments of electrode and electrolyte materials for different types of ASBs, i.e., ARBs, DIBs (including insertion-type, conversion-type, and conversion-insertion-type DIBs), and RDIBs. We also highlight the challenges and prospects of the ASB technology toward future grid energy storage.

SHUTTLE MECHANISMS

The different working principles of ASBs are illustrated in Figure 2. On the basis of the anion-shuttling mechanism, ASBs can be further divided into 3 types: ARBs, DIBs, and RDIBs. As shown in Figure 2A, ARBs, e.g., fluoride-ion batteries and chloride-ion batteries, depend on the electrochemically stable anions as charge carriers.^{9,10} During the discharging process, anions are released from the cathode, shuttle through the electrolyte, and react with the anode material. During charging, the process occurs in reverse. The above electrochemical processes enable high theoretical energy densities, especially considering volumetric energy density, with output voltages of 2–4 V.²¹

In contrast to ARBs, DIBs hinge on both anions and cations being charge carriers. More specifically, DIBs include three types: insertion-type, conversion-type, and conversion-insertion-type. Insertion-type DIBs have been the most common ones so far. In the insertion-type DIBs, anions and cations are simultaneously inserted into or decoupled from electrodes (Figure 2B).²² In DIBs, during the charge process, anions and cations in the electrolyte migrate toward the cathode and anode.

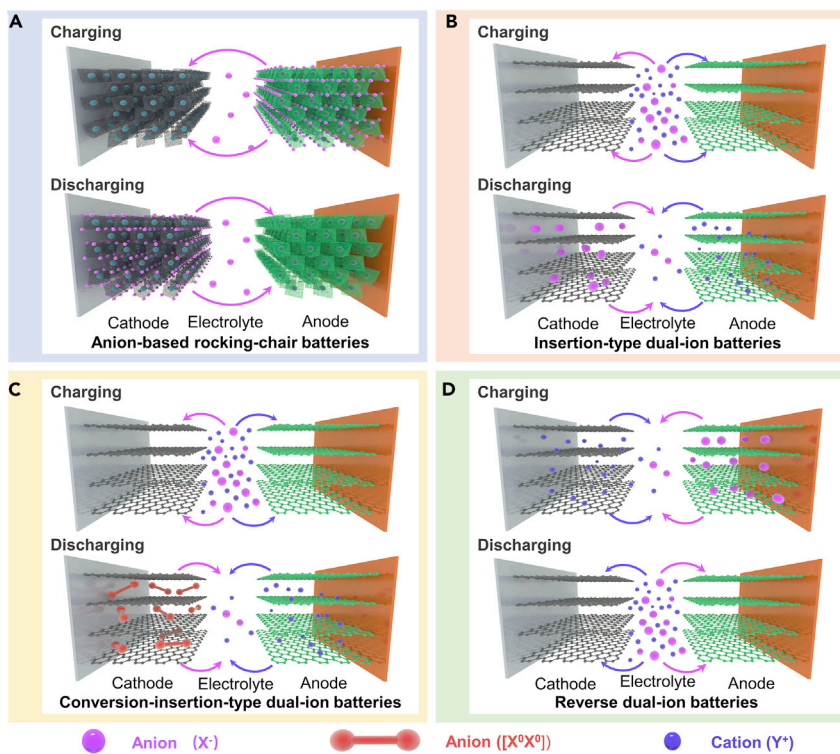


Figure 2. The operational working mechanisms of different ASBs

- (A) ARBs.
- (B) Insertion-type DIBs.
- (C) Conversion-insertion-type DIBs.
- (D) RDIBs.

Conversely, the intercalated anions and cations in electrodes are released into electrolytes during the discharge process. The storage and release of ions are associated with faradic charge storage processes, such as intercalation or de-intercalation reactions in the host materials or anode alloying reactions. In comparison with traditional alkali metal-based batteries, the intercalations of anions into cathode host materials contribute to a higher operating voltage (up to ≈ 5.0 V in the case of graphite cathode), which facilitates to enhanced energy densities.²³ Furthermore, low-cost carbonaceous materials are widely employed as cathode host materials for DIBs. Such transition-metal-free configurations endow DIBs with cost-efficiency and environmental friendliness. Conversion-type DIBs employ conversion reactions of anions at cathode. For instance, zinc-iodine DIBs function via the Zn/Zn^{2+} redox couple on the anode and I_3^-/I^- redox couple on the cathode.²⁴ The Zn^{2+} and I^- ions move from electrolyte to electrodes during the charge process, and they are then released from electrodes into the electrolyte in the subsequent discharge process. Conversion-insertion-type DIBs are a further type of DIBs. Figure 2C displays a schematic diagram of conversion-insertion-type DIBs based on anion shuttling with conversion-intercalation reactions. Such DIBs use a two-step reversible reaction during the charge process: a conversion process of anions occurs first at the cathode, followed by an intercalation of the oxidation products into the electrode. In detail, on the cathode side during the charge process, the conversion process is a single-electron transfer oxidation of halide (X^-) to elemental halogen (X^0) at a low potential. Subsequently, X^0 intercalates into the layered host cathode with the formation of intercalation compounds. Along with this process, cations are inserted into the

anode host materials.²⁵ The discharge reverses the above conversion-intercalation processes (i.e., the intercalated halogen atoms transform back to halides that are released into the electrolytes). This mechanism possesses both the merits of conversion reactions (i.e., high energy densities) and intercalation reactions (i.e., good reversibility), which is promising for the future design of energy-dense batteries.

Similar to DIBs, RDIBs also employ both anions and cations as charge carriers (Figure 2D). However, here the cations are inserted into the anode and anions are inserted into the cathode during the discharging process, while they are simultaneously released into the electrolyte during the charge process. This operation configuration is opposite to that of the DIBs. Unlike the conventional cation-based “rocking-chair” batteries (e.g., Li-ion batteries) where the preferred cation transference number is 1, the ideal cation transference number for DIBs and RDIBs is 0.5, i.e., both anions and cations carry the same electrical conductance.²² As a result, inorganic solid-state electrolytes with higher transference number (close to ≈ 1) are not suitable for DIBs and RDIBs. Furthermore, the salt concentration in the electrolyte plays a key role in the electrochemical processes of DIBs and RDIBs.²⁶ On one hand, during the charge process of DIBs or the discharging process of RDIBs, the salt concentration in the electrolytes reduces during the ion intercalation into the electrodes. Therefore, the salt concentration should be sufficiently high to allow the ion storage in the electrodes.²⁷ On the other hand, high salt concentrations can reduce the amounts of solvents in the electrolyte, which, hence, enables an enhanced energy density.²² However, beyond these positive effects, high salt concentration also leads to high viscosity of the electrolyte, thereby reducing the electrolyte ionic conductivity and increasing the polarization. Therefore, the salt concentration in electrolytes needs to be carefully optimized to balance the energy density, kinetics, and cost.

ARBs

Compared with traditional rechargeable metal-ion batteries (e.g., Li-ion batteries), ARBs present numerous advantages, such as high theoretical volumetric energy density and low cost.²³ Nevertheless, their practical applications are severely limited by the restricted availability of suitable electrode materials and electrolyte. Thus, further optimization of electrode structures and electrolyte compositions is required. In this section, we discuss the anion storage mechanisms of ARBs (e.g., fluoride-ion battery and chloride-ion battery) with different electrolyte systems, i.e., aqueous electrolytes and non-aqueous electrolytes, and comprehensively discuss the recent progress of these ARBs.

Non-aqueous fluoride-ion batteries

Fluoride-ion batteries are attracting great attention because of their high theoretical volumetric energy densities (up to 5,000 Wh L⁻¹, based on the total volume of cathode and anode) when employing metallic anodes (e.g., cerium (Ce), lead (Pb), tin (Sn), Zn, and Li) and metal fluorides (e.g., CuF₂ and BiF₃) or fluoride-forming metal oxides (e.g., LaCoO₄ and LaSrMnO₄) as cathode.²⁸ In the early research stages, inorganic solid-state electrolytes based on fluoride-ion conducting compounds (e.g., La_{0.9}Ba_{0.1}F_{2.9})⁹ were widely applied in fluoride-ion batteries. Given that the ionic conductivities of such solid-state electrolytes are not high enough at room temperature, the resulting solid-state fluoride-ion batteries are generally operated at a relatively high temperature (>150°C).

A proof-of-principle of rechargeable fluoride-ion batteries is demonstrated in Figure 3A.⁹ A full cell was constructed with a conversion-type BiF₃ cathode, a

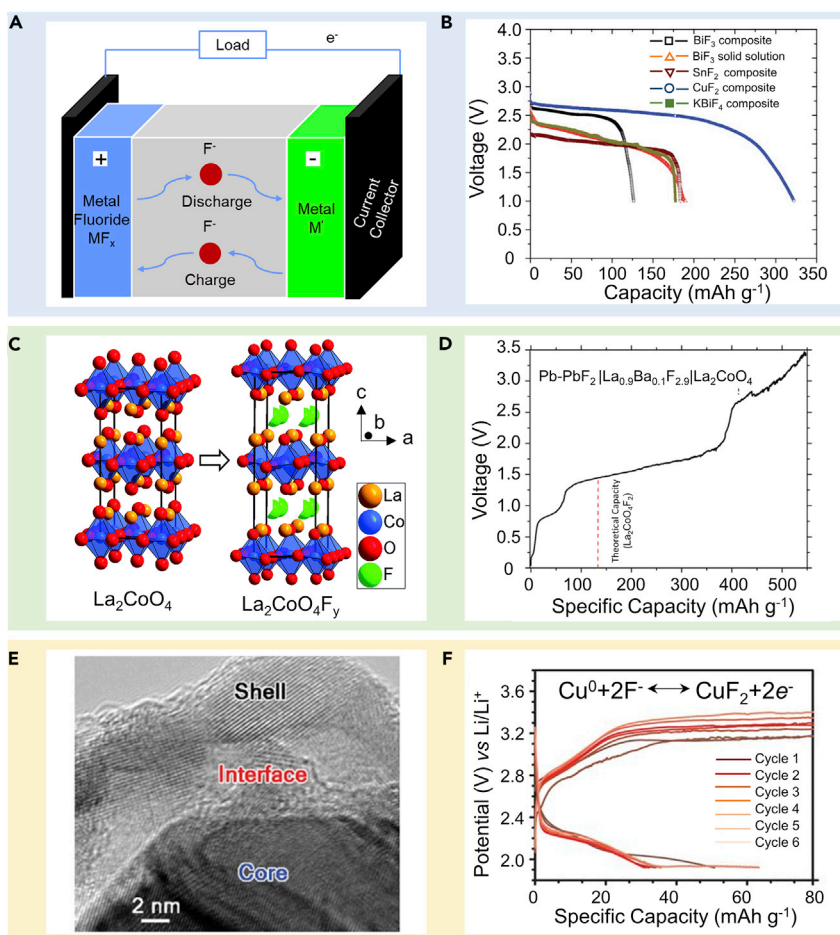


Figure 3. Fluoride-ion batteries

(A and B) Shown are the (A) schematic diagram and (B) corresponding discharging profiles of a rechargeable Ce metal| $La_{0.9}Ba_{0.1}F_{2.9}|M'F_x$ cell at 150°C with a current density of 10 $\mu A\text{ cm}^{-2}$, Reprinted with permission from Reddy et al.⁹ Copyright 2011 Royal Society of Chemistry.

(C and D) Shown is the (C) operating mechanism of intercalation-type La_2CoO_4 cathode in fluoride-ion batteries and the (D) discharge profile of a $Pb-PbF_2|La_{0.9}Ba_{0.1}F_{2.9}|La_2CoO_4$ cell at 170°C with a current density of 10 $\mu A\text{ cm}^{-2}$. Reprinted with permission from Nowroozi et al.³⁰ Copyright 2018 Royal Society of Chemistry.

(E and F) Shown are the (E) TEM image of core-shell $Cu@LaF_3$ and the (F) charge-discharge profile of a three-electrode cell with $Cu@LaF_3$ as the cathode with 1 M NpF in BTFE liquid electrolyte. Reprinted with permission from Victoria et al.³⁸ Copyright 2018 Science Publish Group.

tysonite-type $La_{0.9}Ba_{0.1}F_{2.9}$ solid-state electrolyte, and a Ce metal anode. Its working mechanism is analogous to the “rocking chair” mechanism in Li-ion batteries except that the charge carriers are fluoride ions (F^-). Upon charging, the F^- ions travel through the electrolyte to the cathode side and are subsequently incorporated by the cathode in a conversion reaction. During the discharge process, a reverse reaction occurs at the cathode, and then the F^- ions travel back to the anode. The typical discharge curves of various metal fluorides versus Ce metal are shown in Figure 3B. The redox cathode and anode reactions during cycling are indicated in Equations 1 and 2:



where “MF_x” and “M” represent the metal fluoride or metal oxide fluoride cathode and metallic anode, respectively. Although fluoride-ion batteries have achieved high discharge capacity with evident plateaus, they still suffer from poor cycling performance. Nowroozi et al. reported a reversible conversion mechanism of CuF₂ in the La_{0.9}Ba_{0.1}F_{2.9} solid-state electrolyte system.²⁹ They proposed that Cu diffusion into the electrolyte and side reactions at the anode|electrolyte interfaces were responsible for the capacity-fading behaviors. Besides these effects, the conversion-type electrodes exhibit the poor transport kinetics and reversibility because of repeated chemical bond formation or breaking during the conversion process, accompanied by strong structural reorganization of the atoms. Therefore, optimizing the structure and the compositions of electrodes and electrolytes and deepening the understanding the electrode|electrolyte interfacial behaviors are critical for the further development. Besides, intercalation electrodes, such as La₂CoO₄ and LaSrMnO₄, were developed as cathode materials for fluoride-ion batteries.^{30,31} As shown in Figure 3C, La₂CoO₄ can host approximately 1.2 fluoride ions per formula mass.³⁰ When applied in a Pb-PbF₂|La_{0.9}Ba_{0.1}F_{2.9}|La₂CoO₄ full cell, the discharge profiles exhibited distinct plateau characteristics at various potentials around 0.25, 0.8, 1.3, and 2.8 V at 170°C (Figure 3D). They also found that regulating the cutoff capacity (65 mA h g⁻¹) efficiently avoided irreversible side reactions between carbon conductive additive and cathode active material, thus improving the reversibility of fluoride-ion batteries. The full cell delivered an initially charge capacity of 65 mA h g⁻¹ based on the cathode material with ≈ 50 % capacity retention after 20 cycles.

Beyond La_{0.9}Ba_{0.1}F_{2.9}, other solid-state electrolytes, such as single crystal tyanite (LaF₃) and fluorite (CaF₂), were developed for fluoride-ion batteries.²⁸ Although these crystalline materials exhibit relatively high ionic conductivities ($\approx 10^{-4}$ S cm⁻¹) at room temperature, the complicated and high-cost synthesis methods hinder their practical utilization in fluoride-ion batteries. In addition, the structural transformation to polycrystalline-type materials resulted in decrease of conductivity of the single crystal electrolytes. Several methods, e.g., doping hetero-atoms,³² introducing nano-structuring,³³ constructing thin-film electrolytes,³⁴ and exploiting ternary fluoride electrolyte systems,³⁵ were developed to enhance the ionic conductivity and, therefore, lower the working temperature of such solid-state electrolytes. In 2018, a room-temperature rechargeable fluoride-ion battery was developed based on a tetragonal BaSnF₄ solid-state electrolyte.³⁶ This solid-state electrolyte possesses a high ionic conductivity of $\approx 3.5 \times 10^{-4}$ S cm⁻¹ at room temperature, with fluoride ions as the charge carriers. Two electrochemical cells, Sn|BaSnF₄|BiF₃ and Zn|BiSnF₄|BiF₃, were assembled and tested at various temperatures. The Sn|BaSnF₄|BiF₃ and Zn|BiSnF₄|BiF₃ cells delivered the first discharge capacity of 120 and 56 mA h g⁻¹ at room temperature, respectively, based on the mass of BiF₃, which was, however, followed by fast and irreversible capacity degradation. Nevertheless, at an elevated temperature of 150°C, the Sn|BaSnF₄|BiF₃ cell could maintain high reversible capacity of 138 mA h g⁻¹ after ten cycles. To date, it still remains a challenging task for solid-state fluoride-ion batteries to simultaneously exhibit room-temperature operation and cycling durability.

Replacing solid-state electrolytes with liquid electrolytes is another way to enhance the ionic conductivity of the electrolyte, which also reduces the working temperature of the fluoride-ion batteries. An ionic liquid electrolyte was designed by dissolving an organic fluoride (1-methyl-1-propylpiperidinium fluoride, MPPF) in N, N, N-trimethyl-N-propylammonium bis(trifluoromethanesulfonyl)amide (TMPA-TFSA)-based ionic liquid with a molar ratio of 1:10.³⁷ Although the room-temperature ionic

conductivity of this electrolyte was as high as $\approx 2.5 \times 10^{-3}$ S cm $^{-1}$, the cycling performance of the fluoride-ion cells based on this electrolyte was still limited due to metal dissolution from the cathode. Victoria et al. reported a liquid electrolyte consisting of 1 M N, N, Ntrimethyl-N-neopentylammonium fluoride salt (Np₁F) in bis(2,2,2-trifluoroethyl) ether (BTFE) solvent, which displayed a high ionic conductivity ($\approx 2.8 \times 10^{-3}$ S cm $^{-1}$) comparable with that of liquid electrolytes for Li-ion batteries (i.e., 10^{-3} to 10^{-2} S cm $^{-1}$ at room temperature).³⁸ Besides the high ionic conductivity, this ether-based electrolyte exhibited a wide electrochemical window of ≈ 4.1 V and a robust chemical stability toward the cathode material and the fluoride salt. To mitigate the metal dissolution from the cathode into this electrolyte, a composite cathode material with a core-shell nanostructure, Cu@LaF₃, was further developed (Figure 3E). The thin LaF₃ shell (thickness: ≈ 5 nm) with electrochemical inertness and highly selective fluoride-ion conductivity served as an artificial solid electrolyte interface (SEI), which enabled facile fluoride ion diffusion between the liquid electrolyte and the Cu core and also blocked Cu dissolution into the electrolyte. XRD measurements indicated CuF₂ formation inside the LaF₃ shell and the plasma mass spectrometry of the electrolyte showed no Cu signal within the detection limits of the instrument. Such composite cathodes exhibited highly reversible fluorination-defluorination reactions at room temperature in the abovementioned liquid electrolytes (Figure 3F).

Gel polymer electrolytes in a quasi-solid-state have also been applied in fluoride-ion batteries. Gschwind et al. developed a polyethylene glycol (PEG)-based gel polymer electrolyte with 0.02 m ammonium bifluoride in dimethylcarbonate (DMC) as a plasticizer.³⁹ Such PEG-based electrolytes not only provided high ionic conductivity ($\approx 2.1 \times 10^{-3}$ S cm $^{-1}$) at room temperature and excellent thermal stability (up to ≈ 340 °C) but also efficiently restrained the dissolution of the reaction products from the anode into the electrolyte. A Li metal||BiF₃/C full cell based on this gel polymer electrolyte exhibited a high discharge capacity of ≈ 136 mA h g $^{-1}$ based on the active mass of cathode material. Extensive advances in fluoride-ion batteries are underway to achieve high energy density and compete in properties against traditional Li-ion batteries.

Non-aqueous chloride-ion batteries

ARBs based on chloride-anion shuttling, i.e., chloride-ion batteries, have also been explored, based on a similar mechanism to that of the fluoride-ion batteries. Chloride-ion batteries possess numerous merits including: (1) low cost and sustainability of chloride sources; (2) high theoretical volumetric energy up to 2,500 Wh L $^{-1}$ based on the total electrodes, which is comparable with that of lithium-sulfur batteries¹⁰; and (3) enhanced safety due to the dendrite-free performance of their metallic anodes during cycling.⁴⁰ All these features benefit the sustainability for potential large-scale energy storage applications. The working mechanism of chloride-ion batteries can be described as follows:



where "MCl_x" represents metal chlorides (CoCl₂, BiCl₃, and VCl₃, etc.), metal oxychlorides (FeOCl, BiOCl, and VOCl, etc.), metal hydroxide chlorides (e.g., (Co₃Fe(OH)₈)Cl·1.6 H₂O), or organic chlorides (e.g., polypyrrole chloride (PPyCl), polyaniline (PANI)) as cathode, and "M'" represents highly electropositive metals (Li, Mg or Ca, etc.) as

anode.¹⁰ Currently, chloride-ion batteries generally apply mixtures of chloride-based ionic liquids (e.g., 1-methyl-3-octylimidazolium chloride ([OMIM][Cl]), 1-butyl-1-methyl-piperidinium chloride (PP₁₄Cl)), and low-melting-point co-solvents (e.g., other ionic liquids or carbonate solvents) as the electrolytes.^{41,42} Although rechargeable chloride shuttling is successfully realized in these electrolytes, the associated cathodes have suffered from severe capacity decay during the charging-discharging processes. Poor cycling performance is mainly due to continuous metal dissolution from the cathode into the electrolyte and side reactions between the cathode material and electrolytes, plus irreversible loss of electrode|electrolyte contacts caused by large volumetric expansion of the electrodes during cycling.

The characteristics of various cathode materials of chloride-ion batteries are summarized in **Table S1**. Compared with metal chlorides, metal oxychlorides (e.g., BiOCl,⁴¹ FeOCl,⁴³ and VOCl⁴²) possess higher chemical stability against metal dissolution of cathode, given that the cations have a strong bonding with the Lewis basic O²⁻ anions. The metal oxychlorides generally form layered structures whereby stacked layers combine through van der Waals interactions. The reversible electrochemical mechanism of FeOCl cathode material was revealed in a Li metal||FeOCl cell with 0.5 M PP₁₄Cl in a 1-butyl-1-methylpiperidinium bis(trifluoromethylsulfonyl)imide (PP₁₄TFSI) electrolyte.⁴¹ During the discharge process, chloride ions are first de-intercalated from FeOCl, and subsequently the cathode is converted to FeO. The FeOCl cathode material delivered an initial capacity of 158 mA h g⁻¹. However, the capacity rapidly faded to 60 mA h g⁻¹ after only 5 cycles, mainly because of the loss of electrical contacts between the FeOCl and conductive carbon caused by a large volume expansion or contraction from the phase transformation between FeOCl and FeO. Yu et al. proposed a nano-confined strategy to improve the electrochemical property of FeOCl.⁴³ A thermal decomposition method under mild conditions was used to synthesize the FeOCl/CMK-3 carbon composite, in which FeOCl was well-confined in the mesopores of CMK-3 carbon. The atomic arrangement of FeOCl materials were investigated in depth with an ionic liquid electrolyte consisting of 0.5 M PP₁₄Cl in PP₁₄TFSI before and after cycling, as illustrated in **Figure 4A**. With the CMK-3 confinement, the discharge capacity was increased to 202 mA h g⁻¹ (based on the mass of cathode active material) at 10 mA g⁻¹, and the cycling stability was improved (**Figure 4B**). This was attributed to the enhanced charge transfer, chloride ion diffusion, and controlled volumetric expansion relaxation provided by the nano-confinement effect in the CMK-3. VOCl exhibits a chloride ion shuttling behavior similar to that of FeOCl. When applied in 0.5 M PP₁₄Cl in PC electrolyte (conductivity: $\approx 4.4 \times 10^{-3}$ S cm⁻¹), the high mobility of chloride ions in the intact layered structure enabled a reversible capacity of 113 mA h g⁻¹ at 2 C (1 C = 261 mA g⁻¹) with a Coulombic efficiency of 98% after 100 cycles.⁴²

Recently, layered double hydroxides (LDHs) were demonstrated as a new cathode material for chloride-ion batteries.⁴⁰ A CoFe-Cl LDH (i.e., [Co₃Fe(OH)₈]Cl · 1.6 H₂O) material exhibited a low energy barrier because of its unique topochemical transformation characteristic, which benefited highly reversible insertion or de-insertion of chloride ions in its two-dimensional (2D) diffusion paths. Such super-stable 2D channels seemed to be supported by chloride ions and the interlayer crystallographic water as pillars in the region between the octahedral host layers. During cycling, the redox couples responsible for the electrochemical reactions were Fe²⁺/Fe³⁺ and Co²⁺/Co³⁺, as shown in **Figure 4C**. Li metal||CoFe-Cl test cells with 0.5 M 1-butyl-1-methylpyrrolidinium chloride (BpyCl) in PC and PP₁₄TFSI electrolyte retained a high discharge capacity of 160 mA h g⁻¹ (based on the mass of cathode active material) with a Coulombic efficiency of > 99 % over 100 cycles at

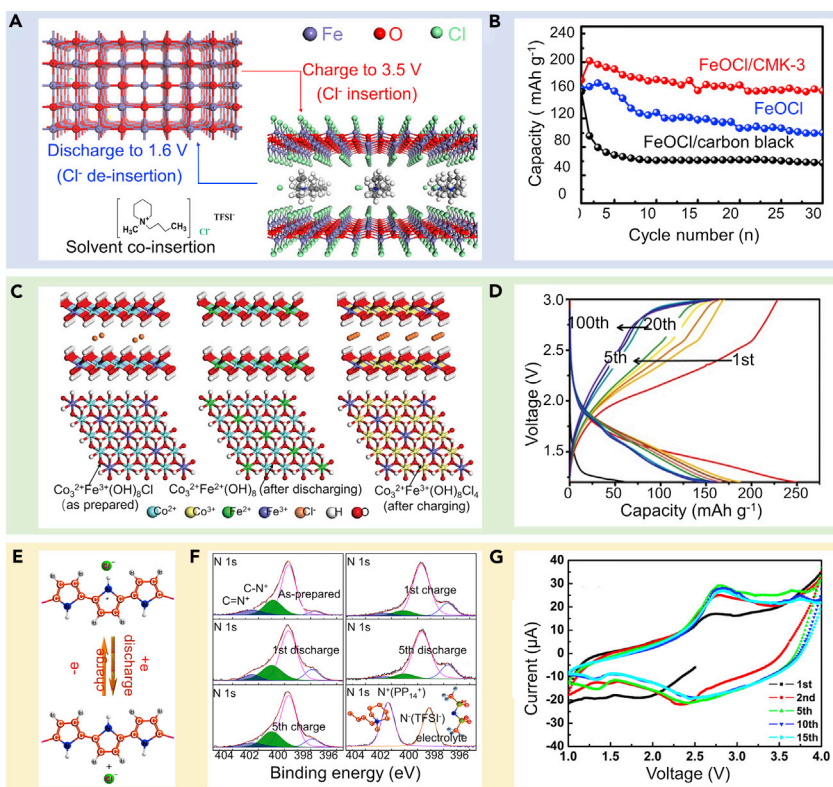


Figure 4. Cathode materials for chloride-ion batteries

(A and B) Shown are the (A) schematic illustration of the electrochemical intercalation process of conversion-type FeOCl material and the (B) cycling performance of various FeOCl composite materials at 10 mA g⁻¹. Reprinted with permission from Yu et al.⁴³ Copyright 2017 American Chemical Society.

(C and D) Shown are the (C) structural representation of CoFe-Cl LDH at various states (from left to right: as-prepared, after discharging and after charging) and the (D) charge-discharge profiles of CoFe-Cl LDH/C composite electrode at 100 mA g⁻¹. Reprinted with permission from Yin et al.⁴⁰ Copyright 2019 Wiley-VCH.

(E–G) Shown are the (E) schematic illustration of electrochemical reactions in PPyCl, (F) N1s XPS spectra of PPyCl@CNT cathodes during cycling and the PP₁₄Cl-PP₁₄TFSI electrolyte, and (G) CV curves of a Li||PPyCl@CNT cell at 50 µV s⁻¹. Reprinted with permission from Zhao et al.⁴⁴ Copyright 2017 American Chemical Society.

100 mA g⁻¹ (Figure 4D). This indicates that LDH materials are promising cathode candidates for halide-based ARBs.

Organic conducting polymers, such as chloride-ion-doped PPyCl and PANI, have also been investigated as cathode materials for chloride-ion batteries.^{44,45} The high chemical and electrochemical stability of these polymeric cathode materials resolved the issues of cathode metal dissolution raised previously. The detailed electrochemical operation mechanism of PPyCl@carbon nanotube (CNT) cathodes is shown in Figure 4E.⁴⁴ The dominant electrochemical reactions were the conjugation of chloride ions with PPyCl based on α - α' linkages during cycling. X-ray photoelectron spectroscopy (XPS, N1s) of PPyCl@CNT cathodes showed a repeated peak intensity change of the N⁺ species during charge-discharge processes (Figure 4F), and cyclic voltammetry (CV) curves remained steady along cycling (Figure 4G). This validates the highly reversible electrochemical reactions claimed for PPyCl@CNT cathodes. The Li metal|0.5 M PP₁₄Cl in PP₁₄TFSI||PPyCl@CNT full cell

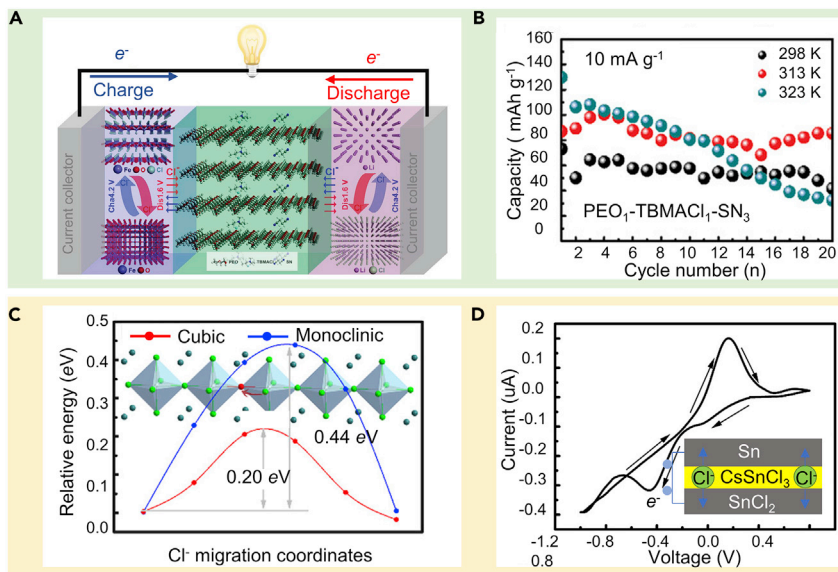


Figure 5. Solid-state electrolytes for chloride-ion batteries

(A and B) Shown are the (A) schematic diagram of a solid-state Li||FeOCl chloride-ion cell with PEO₁-TBMACl₁-SN₃ polymer electrolyte and the (B) corresponding cycling performance at 10 mA g⁻¹. Reprinted with permission from Chen et al.^[46] Copyright 2019 Wiley-VCH.

(C and D) Shown are the (C) theoretical energy barrier of chloride ion migration in inorganic halide perovskites and the (D) CV curves of a SnCl₂|cubic CsSnCl₃|Sn cell at 50 μ V s⁻¹ at 40°C. Reprinted with permission from Xia et al.^[47] Copyright 2020 American Chemical Society.

yielded an initial discharge capacity of 93 mA h g⁻¹ with a relatively low median voltage value of \approx 2.4 V at 10 mA g⁻¹, which was 80% of the theoretical capacity (i.e., 115 mA h g⁻¹, based on a doping level of 0.33 (PPyCl_{0.33})). These relative low energy densities limit the practical application of polymeric cathodes. A combination of polymeric cathodes with inorganic cathodes, to achieve a balance between energy density and cycling stability, could be a potential research direction for the future development of chloride-ion batteries.

Chloride-ion-conducting solid-state or quasi-solid-state polymer electrolytes have been developed to solve the issue of cathode metal-ion dissolution, which is serious in chloride-ion batteries based on ionic liquid-based electrolytes.¹⁰ Gschwind et al. investigated the electrochemical behaviors of gel polymer electrolytes on the basis of polyvinyl chloride (PVC), commercial gelatin, or polyvinylidifluoride-hexafluoropolymer (PVDF-HFP) as the polymer matrices.⁴⁵ The Zn||CuCl₂/C cell showed the best electrochemical performance with the gel polymer consisting of gelatin, tetraethylammonium chloride (TEACl), and dimethylsulfoxide (DMSO). Soon after, Chen et al. constructed a rechargeable solid-state chloride-ion battery based on polyethylene oxide (PEO) as polymer matrix and tributylmethylammonium chloride (TBMACl) as chloride ion source (Figure 5A).⁴⁶ Succinonitrile (SN) was employed as a solid plasticizer to further enhance the ionic conductivity of solid polymer electrolyte. This polymer electrolyte exhibited an ionic conductivity of \approx 10⁻⁵ S cm⁻¹ at 25°C. The as-assembled solid-state Li metal||FeOCl cell displayed reversible electrochemical redox reactions with discharge capacities of about 60, 90, and 40 mA h g⁻¹ (based on the active mass of FeOCl) at 298, 313, and 323 K, respectively (Figure 5B).

Inorganic solid-state electrolytes are also available for chloride-ion batteries. Xia et al. reported a room-temperature stable inorganic halide perovskite, cubic

CsSnCl_3 , as a potential solid-state electrolyte for chloride-ion batteries.⁴⁷ As shown in Figure 5C, the migration energy barrier of cubic CsSnCl_3 (0.20 eV) is much lower than that of monoclinic CsSnCl_3 (0.44 eV) according to density functional theory (DFT) calculations. Consequently, cubic CsSnCl_3 shows an improved ionic conductivity ($\approx 3.6 \times 10^{-4} \text{ S cm}^{-1}$ at room temperature) compared with that of the monoclinic CsSnCl_3 ($\approx 10^{-9} \text{ S cm}^{-1}$ at room temperature). In the CV pattern of a Sn|cubic $\text{CsSnCl}_3|\text{SnCl}_2$ cells at 40°C, no peaks related to electrolyte decomposition were observed, demonstrating the high electrochemical stability of this electrolyte (Figure 5D). Further improvement in ionic conductivities for the solid-state electrolytes is still required to accomplish a room-temperature operation of the solid-state chloride-ion batteries.

On the anode side, most studies of chloride-ion batteries employed Li metal as the anode. Replacing Li metal with other abundant metals (e.g., Na, Mg, and Ca) as the anode will undoubtedly reduce the cost of chloride-ion batteries.⁴⁸ In particular, Mg metal could be a promising anode for chloride-ion batteries because of its low cost and ability to provide two electrons per redox reaction. Considering the electrolyte decomposition products on the surface of pure Mg anode block the reversible plating-stripping of Mg, a Mg/C composite anode was developed to mitigate interfacial side reactions.⁴⁹ The Mg/C anode-based chloride-ion cells with FeOCl or BiOCl as cathode and 0.5 M PP_{14}Cl in $\text{PP}_{14}\text{TFSI}$ as electrolyte deliver the initial discharge capacity of 102 and 130 mA h g^{-1} , respectively, (based on the mass of cathode active material) at 10 mA g^{-1} . However, the cells still suffer from a large capacity decay upon cycling because of the volumetric expansion of Mg and the residual interfacial side reactions. Therefore, it remains a huge challenge to develop suitable non-Li metal anode for high-performance chloride-ion batteries.

Other non-aqueous halide-based rocking-chair batteries

Non-aqueous bromide-ion batteries have been reported for energy storage.⁵⁰ As a proof-of-concept, Yin et al. reported a bromide-ion battery constructed with Li metal as anode, the bromide-intercalated CoNi LDH as cathode, and 0.5 M 1-butyl-1-methylpyrrolidinium bromine (Bpy_{14}Br) dissolved in PC as the electrolyte.⁵⁰ *Ex situ* XRD, XPS, and energy-dispersive X-ray spectroscopy (EDS) measurements verified that bromide ions could be reversibly inserted or de-inserted into/from the LDH cathode, meanwhile a valence change of Co/Ni was observed with minimal structural or morphological change in the LDH domain. The as-prepared LDH cathode material possessed a maximum discharge capacity of 338.9 mA h g^{-1} with a plateau at a potential of $\approx 1.7 \text{ V}$ and a stable reversible capacity of $\approx 100 \text{ mA h g}^{-1}$ (based on the mass of LDH) after 50 cycles at 200 mA g^{-1} . This demonstrates the utilization potentiality of the bromide-ion batteries.

Besides halide ions, metal-halide complex ions (hereafter referred to as superhalides) have also been applied to develop high-performance ARBs. For example, Lin et al. reported an ARB with chloroaluminate (AlCl_4^-) anions as charge carriers during cycling.⁵¹ Their ARB contained Al metal as the anode, flexible graphitic foam as the anode, and AlCl_3 in 1-ethyl-3-methylimidazolium chloride (EMIMCl) as the electrolyte. At the anode, Al metal and AlCl_4^- react to form Al_2Cl_7^- during discharging, and a reverse reaction occurs during charging. At the cathode, AlCl_4^- anions are intercalated or de-intercalated between graphite layers during charge and discharge processes, respectively. Full cells delivered a specific capacity of about 70 mA h g^{-1} (based on the mass of graphite cathode) and a high Coulombic efficiency of approximately 98% at 66 mA g^{-1} and lasted for more than 7,500 cycles at 4,000 mA g^{-1} without obvious capacity decay. Further optimizations on this

battery system mainly focused on engineering the graphite cathode structures⁵² and employing gel polymer electrolytes to enlarge the electrolyte electrochemical window.⁵³ Expanding the superhalide-shuttling chemistry is attractive for the development of cost-effective, safe, and high-power-density batteries for safer grid energy storage.

Aqueous ARBs

As discussed so far, organic liquid electrolytes with flammable and/or toxic solvents are extensively employed in most ARBs. Compared with these organic liquid electrolytes, aqueous electrolytes exhibit conspicuous advantages, including non-flammability, eco-friendliness, and cost benefits due to the non-reliance on ultra-dry manufacturing facilities at cell, module, or pack levels.⁵⁴ However, most of the electrode materials for ARBs suffer from low compatibility or severe dissolution in aqueous environments. Therefore, the development of aqueous ARBs necessitates screening of appropriate redox couples.

Rechargeable aqueous alkaline cells have been developed with oxides,⁵⁵ hydroxides,⁵⁶ or sulfides as cathode,⁵⁷ Zn or iron (Fe) metals as anode, and hydroxide ions (OH^-) as charge carriers in the electrolytes. This proof-of-concept was proposed from "Edison batteries" with nickel oxyhydroxide (NiOOH) and Fe as cathode and anode, respectively.⁵⁸ More recently, Parker et al. reported an aqueous $\text{NiOOH}||\text{Zn}$ cell with an anode reaction of $\text{Zn} + 4 \text{OH}^- \leftrightarrow [\text{Zn}(\text{OH})_4]^{2-} + 2\text{e}^-$ and a cathode reaction of $\text{NiOOH} + \text{H}_2\text{O} + \text{e}^- \leftrightarrow \text{Ni}(\text{OH})_2 + \text{OH}^-$.⁵⁶ At a deep depth of discharge, this battery delivered a specific energy competitive to that of commercial Li-ion batteries and exhibited a lifespan of more than 50,000 cycles with a preset voltage limit of 0.8 V. This illustrates its high reliability and promising application potential.

Halide ions can be reversibly stored in silver (Ag) and bismuth (Bi)-containing electrodes on the basis of a conversion mechanism.⁵⁹ In 2017, a rechargeable chloride-ion battery was designed by using BiOCl as the anode, Ag metal as the cathode, and 1 M NaCl aqueous electrolyte.¹⁴ As displayed in Figure 6A, upon charging, chloride ions travel through the aqueous electrolyte from the anode side ($3\text{BiOCl} + 3\text{e}^- \rightarrow \text{Bi} + \text{Bi}_2\text{O}_3 + 3\text{Cl}^-$, where Bi and Bi_2O_3 are the decomposition products of unstable BiO) to the cathode side ($\text{Ag} + \text{Cl}^- \rightarrow \text{AgCl} + \text{e}^-$), whereas the opposite process reversibly occurs upon discharging. This aqueous chloride-ion cell delivered a highly stable discharge capacity of 92 mA h g^{-1} (based on the mass of BiOCl) with a Coulombic efficiency of $\approx 99\%$ after 40 cycles at a current rate of 400 mA g^{-1} (Figure 6B). Besides this material, $\text{Sb}_4\text{O}_5\text{Cl}_2$ has also been applied as an anode material in chloride-ion batteries with aqueous NaCl electrolyte.⁶⁰ When assembled with an Ag cathode in a 1 M NaCl aqueous electrolyte, the full cell maintained a discharge capacity of 34.6 mA h g^{-1} (based on the mass of $\text{Sb}_4\text{O}_5\text{Cl}_2$) after 50 cycles at 600 mA g^{-1} . This aqueous battery model provides a prospect of employing seawater as the electrolyte for rechargeable batteries.

Fluoride ions possess excellent merits, such as superior electrochemical stability, small size, and light weight, which benefits charge transport when applied as charge carriers in rechargeable ARBs. Recently, an aqueous fluoride-ion flow battery was proposed in 2019.¹³ The cell was constructed with a 0.8 M NaF aqueous electrolyte ($\approx 5.173 \times 10^{-4} \text{ S cm}^{-1}$ at room temperature) coupled with a 4-hydroxy-2,2,6,6-tetramethylpiperidin-1-oxyl (4-hydroxy-TEMPO) cathode and a BiF_3 anode (Figure 6C). An anion exchange membrane (AEM) allowed the transport of fluoride ions between the anode and cathode for balancing the charge. This flow battery displayed specific

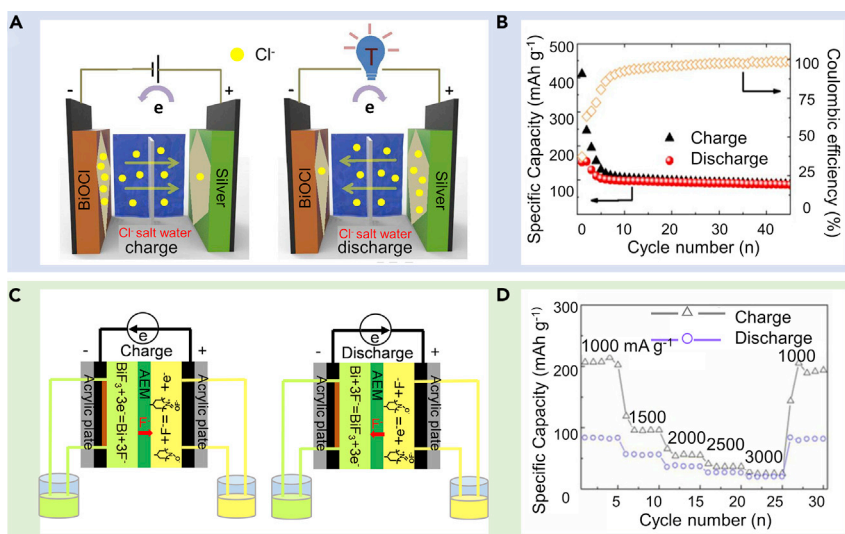


Figure 6. Aqueous anion-shuttle rocking-chair batteries

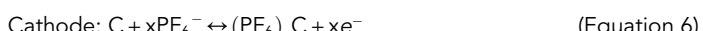
(A and B) Shown are the (A) schematics of a $\text{BiOCl} \mid 1 \text{ M NaCl}$ aqueous electrolyte|Ag chloride-ion cell upon cycling and the (B) corresponding cycling performance at 400 mA g^{-1} . Reprinted with permission from Chen et al.¹⁴ Copyright 2017 Elsevier.

(C and D) Shown are the (C) schematics of an aqueous 4-hydroxy-TMPO|0.8 M NaF salt aqueous electrolyte| BiF_3 fluoride-ion flow cell upon cycling and the (D) rate performance of this cell. Reprinted with permission from Hou et al.¹³ Copyright 2019 Elsevier.

discharge capacities of 83 mA h g^{-1} , 56.2 mA h g^{-1} , 38 mA h g^{-1} , 26.3 mA h g^{-1} , and 19.4 mA h g^{-1} (based on the mass of BiF_3) at current rates of $1,000$, $1,500$, $2,000$, $2,500$, and $3,000 \text{ mA g}^{-1}$, respectively (Figure 6D). Despite the safety and environmental friendliness merits, the energy density of state-of-art aqueous ARBs still needs to be improved via innovations in electrolyte-compatible electrode materials.

INSERTION-TYPE DIBs

DIBs operate based on the electrochemical reactions of both cations and anions. Insertion-type DIBs are the most studied DIBs. Typically, the electrochemical reactions occurring on the electrodes in graphite-based insertion-type DIBs (e.g., PF_6^- and Li^+ as active ions) can be summarized by Equations 5 and 6²⁷



Compared to traditional metal-ion batteries, the reactions occurring on DIB cathodes are the insertion and withdrawal of anions rather than cations.²² In this regard, DIBs can achieve several huge advantages, including low cost, high output voltage, and environmental friendliness. However, the high operation voltage and repeated intercalation or deintercalation of large-radius anions can trigger electrolyte decomposition and structural deterioration of cathode materials.⁶¹ Therefore, for the purpose of stable electrochemical performance, it is of great importance to develop suitable anion hosts and appropriate electrolytes for DIBs. In this section, we discuss the intercalating or de-intercalating mechanisms of anions in insertion-type DIB cathodes in detail and systematically summarize the recent progress in insertion-type DIBs based on different anion host materials (e.g., graphite) and various electrolyte systems (e.g., aqueous electrolytes and non-aqueous electrolytes).

Graphite-based non-aqueous insertion-type DIBs

Graphite with low cost and a stable layered structure is the most widely investigated anion host material (i.e., cathode) for insertion-type DIBs. Until now, the mechanisms of various anions inserting into graphite have been reported, including PF_6^- ,⁶² bis(trifluoromethanesulfonyl) imide anion (TFSI⁻),⁶³ and bis(fluorosulfonyl) imide anion (FSI⁻).⁶⁴ Generally, the intercalation of these anions into graphite occurs at relatively high voltages (e.g., ≈ 4.5 V versus Li/Li⁺ in Li-based DIBs); therefore, high-voltage stability is indispensable for their electrolytes. Such highly stable electrolytes can be designed by optimizing their composition, e.g., adding additives,²³ employing fluoride solvent-based electrolytes,⁶⁵ and increasing the salt concentration of electrolytes.⁶⁴

When anions intercalate into the layered structure of graphite, graphite turns into a graphite intercalation compound (GIC). Compared to pristine graphite, the interlayer distance in GICs is enlarged, meanwhile the interlayer interactions among the graphene layers are weakened. This intercalation mechanism has been explained by two models: the Rüdorff model and the Daumas-Hérolde model (Figure 7A).⁶⁶ Rüdorff model illustrates that no structural distortion of the graphene layers occurs during insertion of ions into the graphite. On the contrary, Daumas-Hérolde model supposes that the graphene layers are flexible and can deform when ions are intercalated.⁶⁷ Assuming that the intercalants are inserted into graphite in a continuous process and there are no defects in the graphite lattice, the formation of GICs can be divided into several stages involving different interlayer spacings. Diffraction techniques, e.g., XRD, can measure the interlayer spacing of graphite and, thus, identify whether anions are inserted into the graphite or not.⁶¹ The structure and particle size of graphitic cathode materials have significant effect on the room-temperature performances of DIBs but little effect on their elevated-temperature performances. Placke et al. investigated the electrochemical performances of 14 types of graphitic materials in TFSI anion-based DIBs.⁶⁸ Among them, mesocarbon microbead (MCMB) delivered the lowest capacity at 20°C, which could be ascribed to the fact that its surface coating hinders the intercalation of TFSI anions. Moreover, graphite with relatively smaller particle size and larger surface area could deliver higher discharge capacity at 20°C. However, these graphite materials with different sizes and structures yielded similar capacity (≈ 100 mAh g⁻¹) at 60°C. It indicates that the improved mobility kinetics of TFSI anions could mitigate the impact of structure and particle size of graphite cathode materials at an elevated temperature.

Among various insertion-type DIBs employing graphite cathodes, Li-based DIBs (with Li-ion as the active cation in the electrolyte) have been investigated in detail. Graphite cathodes can be coupled with various anodes for Li-based DIBs, including graphite,⁶⁵ amorphous carbon,⁶⁹ Li metals,⁷⁰ Si,⁷¹ and even bare Al foil.⁷² A Li-based DIB was reported applying graphite as both cathode and anode materials.⁶⁵ With 1.7 M LiPF₆ and 5 mM tris(hexafluoro-iso-propyl)phosphate (HFIP) additive in an electrolyte of fluoroethylene carbonate (FEC):ethyl methyl carbonate (EMC) (4:6 by weight), the as-developed DIB enabled a reversible intercalation or deintercalation of PF_6^- into graphite cathode and achieved a high operation voltage of 5.2 V. Such cell delivered a specific capacity of 60 mA h g⁻¹ at 1/7 C, which decayed 0.75% per cycle in 50 cycles. Establishing a stable and robust cathode electrolyte interface (CEI) layer on the graphite cathode can further enhance the structural stability of graphite during battery operation and, thus, improve the cycling performances of DIBs. Artificial CEI layers have been reported to modify graphite cathodes for Li-based DIBs (Figure 7B).⁷⁰ Such artificial CEI layers were generated by a 5-cycle

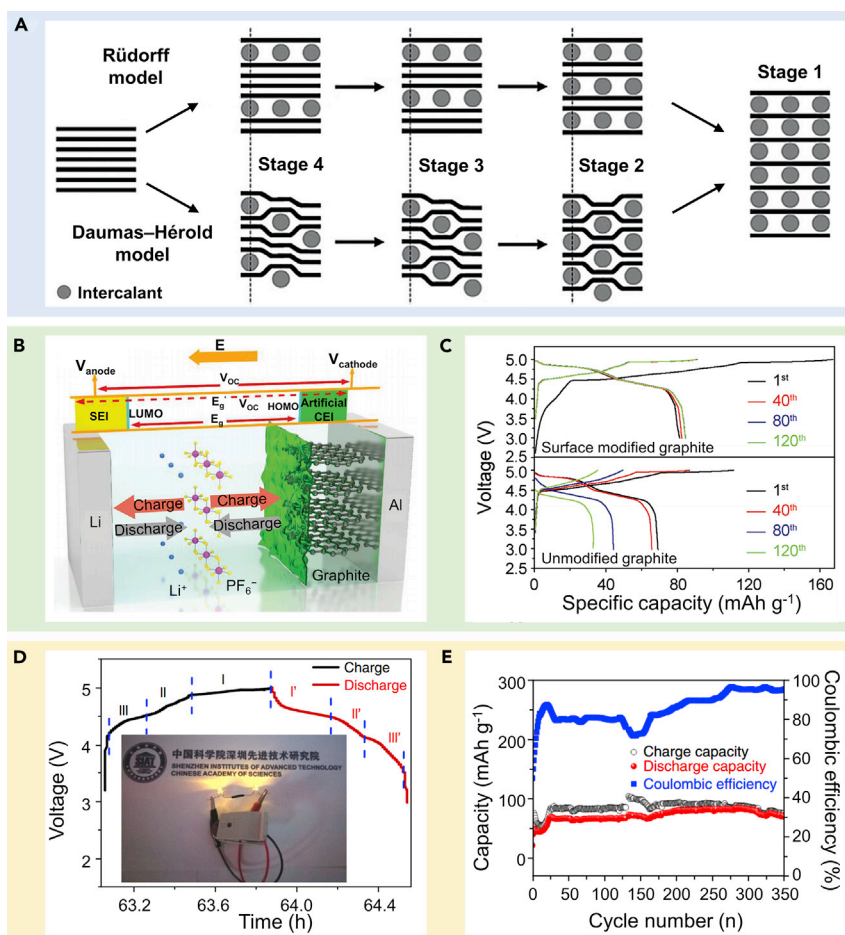


Figure 7. Insertion-type DIBs based on graphite cathodes and organic liquid electrolytes

(A) Schematic illustration of ion intercalation into graphite according to different models.

Reprinted with permission from Sole et al.⁶⁷ Copyright 2014 Royal Society of Chemistry.

(B and C) Shown are the (B) scheme illustration showing the Li-based DIBs with an artificial CEI on the graphite cathode and the (C) typical charge-discharge curves of Li-based DIBs with modified graphite cathode and unmodified cathode at 200 mA g^{-1} . Reprinted with permission from Li et al.⁷⁰ Copyright 2018 Wiley-VCH.

(D and E) Shown are the (D) Typical charge-discharge curves of Ca-based DIB with graphite cathode; the inset is one such cell driving two LEDs in series and the (E) cycling stability of such Ca-based DIB at 100 mA g^{-1} . Reprinted with permission from Wang et al.⁷⁶ Copyright 2018 Nature Publishing Group.

galvanostatic charge-discharge process at a relatively small current rate of 100 mA g^{-1} (based on the active mass of graphite cathode) and in a relatively low potential range (0.3–2.0 V versus Li/Li^+) in a 1 M LiPF_6 in EMC electrolyte. This artificial CEI layer limited electrolyte decomposition and solvation effects of anions near the surface of the graphite cathode, and thus improved the stability of graphite cathode during cycling. As a result, when the upper voltage limit was set at 5 V, the Li metal||as-modified graphite DIB delivered a higher capacity of 80 mA h g^{-1} and much better cycling stability at 200 mA g^{-1} than cells with non-treated graphite cathodes (Figure 7C). Furthermore, highly concentrated electrolytes are reported to improve the cycling stability of graphite cathodes.⁶⁴ Compared to electrolytes with 4 M lithium bis(fluorosulfonyl)imide (LiFSI), the more concentrated 7.5 M LiFSI in EC: DMC (1:1 by volume) electrolyte expanded the electrolyte oxidation stability

from 4.9 to 6.0 V versus Li/Li⁺ and enabled DIBs to attain much better cycling stability to 300 cycles.⁶⁴ In addition, given that applying highly concentrated electrolyte can decrease the total amount of electrolyte solvent required, the overall energy density of the battery can be improved. Using aluminum foil as an alloying anode and graphite as cathode, such a DIB yielded an energy density of 180 Wh kg⁻¹ based on the total mass of electrode active materials and electrolyte.

To further reduce the cost of insertion-type DIBs, non-Li-based DIBs (e.g., Na-,⁷³ K-,⁷⁴ Zn-,⁷⁵ and Ca-⁷⁶ based DIBs) with graphite cathodes have received great research attention in recent years. The applications of these earth-abundant elements can further reduce the cost of DIBs.⁷⁷ Recently, a Ca-based DIB was reported with graphite as cathode and Sn foil as anode.⁷⁶ As shown in Figure 7D, three plateau regions in the charge-discharge profiles indicate different consecutive transformations of graphite during PF₆⁻ insertion. The high output voltage of such a cell successfully powered two light-emitting diodes (LEDs) in series (Figure 7D, inset). A 0.8 M Ca(PF₆)₂ in EC: PC: DMC: EMC (2: 2: 3: 3 by volume) electrolyte was determined to be a stable electrolyte for Ca-based DIBs. As a result, the as-fabricated DIBs delivered a specific capacity of 80 mA h g⁻¹ (based on the weight of the graphite cathode) after 350 cycles at 100 mA g⁻¹ with almost no capacity decay (Figure 7E). It should be noted that the capacity and Coulombic efficiency of such Ca-based DIB was increasing during the cycling test, which could be ascribed to a continuous activation process. Furthermore, a novel Zn-based DIB was constructed with the addition of trimethyl phosphate solvent in 1.5 M Zn(TFSI)₂ in EMC electrolyte, which enabled the operation of a 2.80 V Zn metall|graphite DIB.⁷⁸ In such electrolyte, a unique anion solvation reconfiguration enabled the anode stability of carbonate electrolytes. The assembled Zn-based DIBs exhibited a long cycle life with 92% capacity retention after 1,000 cycles.

Considering that organic liquid electrolytes still face leakage and flammability issues, insertion-type DIBs employing non-flammable quasi-solid-state electrolytes have been investigated to enhance battery safety.⁷⁹ In addition, employing quasi-solid-state electrolytes with crosslinking polymer matrices can effectively regulate cation or anion fluxes, thus enabling homogeneous ion intercalation (or deposition) into or onto the electrodes. An *in situ* synthesized gel polymer electrolyte was developed for Na metall|graphite DIBs, in which ethoxylated pentaerythritol tetraacrylate (EPTA) monomers were selected to gelate a PC:EMC: FEC (1:1:1 by volume) electrolyte containing 0.5 M NaPF₆ and 4 wt% panesultone (PS) additive.⁷⁹ In such a gel polymer electrolyte, FEC formed a robust SEI layer on the Na metal anode, whereas PS assisted to generate a thin CEI layer on the graphite cathode (Figure 8A). *In situ* XRD results confirmed the good reversibility of PF₆⁻ (de)intercalation into the graphite cathode (Figure 8B). Based on the mass of graphite cathode alone, this gel polymer electrolyte-based DIB yielded a specific energy of 484 Wh kg⁻¹ with an output voltage of \approx 4.4 V. During cycling, such cells delivered capacities of \approx 78 mA h g⁻¹ after 1,000 cycles at 100 mA g⁻¹, indicating their excellent cycling stability. Recently, a novel gel polymer electrolyte was developed based on graphene oxide and a PEO co-modified PVDF-HFP polymer framework for Li-based DIBs.⁸⁰ In this gel polymer electrolyte, graphene oxide, PEO, and PVDF-HFP formed hydrogen bonds between each other, which led to a disarranged polymer structure with a porous polymer morphology and decreased PEO crystallinity, which effectively facilitated ion transfer in the electrolyte. After soaking the copolymer in 4 M LiPF₆ in EMC with 2% vinylene carbonate (VC) liquid electrolyte, this as-prepared gel polymer electrolyte showed a high ionic conductivity up to \approx 2.1 \times 10⁻³ S cm⁻¹ at room temperature. When employed as a quasi-solid-state

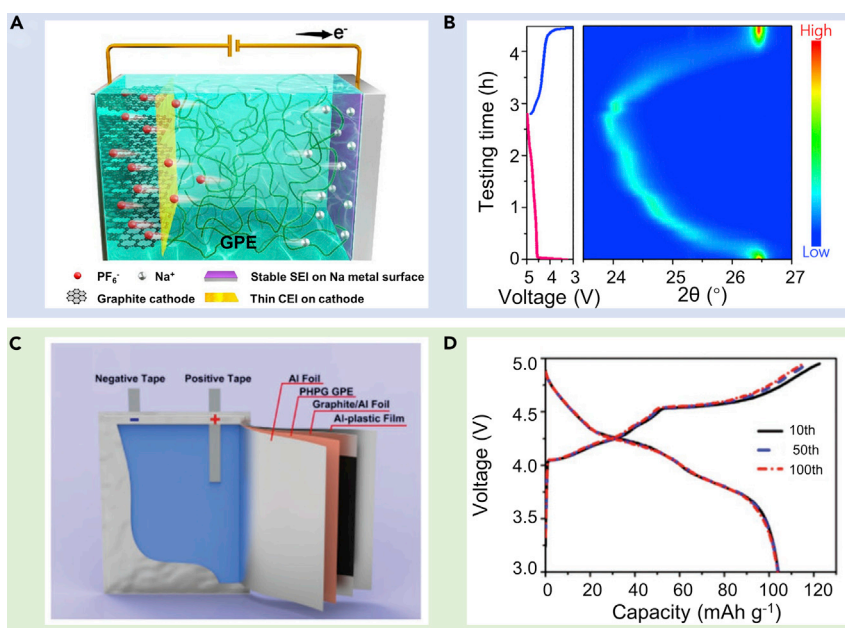


Figure 8. Insertion-type DIBs based on graphite cathodes and quasi-solid-state electrolytes

(A and B) Shown are the (A) schematic illustration of the Na-based DIB using a gel polymer electrolyte and the (B) intensity contour map derived from *in situ* XRD profiles of the Na|gel polymer electrolyte|graphite cell during the initial discharge and charge process at 10 mA g⁻¹. Reprinted with permission from Xu et al.²³ Copyright 2020 Elsevier.

(C and D) Shown are the (C) schematic illustration showing the structure of the soft-packaged DIB based on a gel polymer electrolyte and the (D) charge-discharge profiles of such DIB at 2 C. Reprinted with permission from Chen et al.⁸⁰ Copyright 2018 Wiley-VCH.

electrolyte to assemble a soft-packaged DIB (Figure 8C), the resultant pouch cell exhibited good flexibility and excellent electrochemical performance and delivered a stable capacity of ≈ 103 mA h g⁻¹ at a current rate of 200 mA g⁻¹ (Figure 8D).

In addition, the characteristics of anion intercalation into graphite in the presence of ionic liquid-based electrolytes have been investigated in recent years.⁸¹⁻⁸³ Ionic liquids generally present high chemical stability, low vapor pressure, and non-flammability features; therefore, they can withstand the high operation voltages of DIBs and greatly enhance battery safety.⁸⁴ For example, 1 M lithium bis-trifluoromethanesulfonimide (LiTFSI) in N-butyl-N-methylpyrrolidinium bis-trifluoromethanesulfonimide (Pyr₁₄TFSI) was employed as the electrolyte for a graphite||graphite DIB.⁶³ Although the 1 M LiTFSI in Pyr₁₄TFSI electrolyte showed a low compatibility with graphite anodes, the addition of a small amount (2 wt%) of ethylene sulfite as a SEI-forming additive successfully enabled the stable operation of the graphite||graphite DIB in such an ionic liquid-based electrolyte. Because of the high stability of ionic liquids, the cells could be reversibly charged to a high cutoff voltage of ≈ 5.2 V. The as-developed battery yielded a stable specific capacity of 50 mA h g⁻¹ based on the mass of graphite cathode and a Coulombic efficiency of 99.8% throughout 500 cycles at 500 mA g⁻¹. Furthermore, the AlCl₄⁻ superhalide was successfully intercalated into graphite in an EMIMCl: AlCl₃ ionic liquid electrolyte.⁸⁵ An in-depth understanding of the AlCl₄⁻ intercalation mechanism was gained by employing energy-dispersive-XRD (ED-XRD) and tomography, where the AlCl₄⁻ intercalation in graphite was observed to proceed on a multi-staged path. The new insight on such mechanisms evidenced a mixed-staged region in the initial phase and a two-staged region in the

second phase, which is of fundamental importance for the future development of AlCl_4^- -based DIBs. However, it should be noted that the cost and viscosity of prevailing ionic liquids are relatively high; therefore, further optimization of ionic liquid systems is important for futuristic viable applications in large-scale energy storage.

Non-graphite-based non-aqueous insertion-type DIBs

A variety of non-graphitic cathode materials have also been developed for insertion-type DIBs, including organic materials,⁸⁶ layered metal oxides,⁸⁷ and metal organic frameworks (MOFs).⁸⁸ These possess different mechanisms for accommodating anions.

Until now, various redox-active organic materials have been reported for insertion-type DIBs, including nitrogen-containing aromatic compounds,⁸⁶ porphyrin-based materials,⁸⁹ and hydrocarbon materials.⁹⁰ Generally, organic materials accommodate anions in a lower voltage range than graphite. This characteristic eases the requirement for high oxidation stability of the electrolytes for DIBs, thus benefiting accessibility to a wider range of electrolytes in DIBs.⁹¹ For example, polytriphenylamine (PTPAn) was synthesized as a cathode material for K-based DIBs.⁹² Figure 9A indicates the mechanisms of such an organic molecule accepting anions during charging and releasing them during discharging. The nitrogen atom in the middle of the triphenylamine unit loses one electron during the charging process to become positively charged, subsequently this nitrogen atom can bind one PF_6^- molecule. As a result, with an additive-free 0.8 M KPF_6 in EC:DEC (1:1 by volume) electrolyte, the PTPAn||graphite full-cell DIB delivered good electrochemical performance within 1.0–4.0 V (Figure 9B).

Layered metal oxides can store anions through an intercalation mechanism, which is similar to that of graphite.⁸⁷ Layered metal oxides, such as $\text{Na}_{0.5}\text{Ni}_{0.25}\text{Mn}_{0.75}\text{O}_2$, were developed as the cathode material for insertion-type DIBs.⁸⁷ As shown in Figure 9C, upon charging, Na ions were de-intercalated from the metal oxide cathode, and ClO_4^- ions were subsequently intercalated into the cathode. The reverse reactions occur during the discharge process. Figure 9D shows charge-discharge curves of a Na metal|| $\text{Na}_{0.5}\text{Ni}_{0.25}\text{Mn}_{0.75}\text{O}_2$ DIB at 20 mA g^{-1} based on the cathode material mass and the cycling performance at 50 mA g^{-1} . These results indicate that such layered metal oxides deliver a high reversibility when storing and releasing anions.

MOFs are a type of organic-inorganic hybrid materials with intramolecular pores, formed by coordination-bond self-assembly of organic ligands and inorganic metal ions or clusters. Their unique and tunable pore structures can effectively accommodate other ions, which makes them promising as insertion-type DIB cathode materials.⁹³ Aubrey et al. prepared a Fe-based MOF, $\text{Fe}_2(\text{dobpdc})$ (dobpdc^{4-} = 4,4'-dioxidobiphenyl-3,3'-dicarboxylate), and found that anions (BF_4^- , PF_6^- , TFSI^- , etc.) can be successfully inserted into this MOF (Figure 9E).⁸⁸ This MOF was subsequently applied as a cathode material to assemble DIBs with Na metal anodes. With 0.6 M NaPF_6 in an EC:DMC electrolyte, the as-developed cell yielded a stable capacity of $\approx 90 \text{ mA h g}^{-1}$ for 50 cycles at 140 mA g^{-1} based on the mass of the MOF cathode (Figure 9F).

Although the various cathode materials detailed above have proved to have the ability to accommodate anions, there is still lack of satisfying cathode materials simultaneously possessing high capacity, good redox kinetics, and high stability for insertion-type DIBs. Furthermore, the mechanisms of anion hosting in these

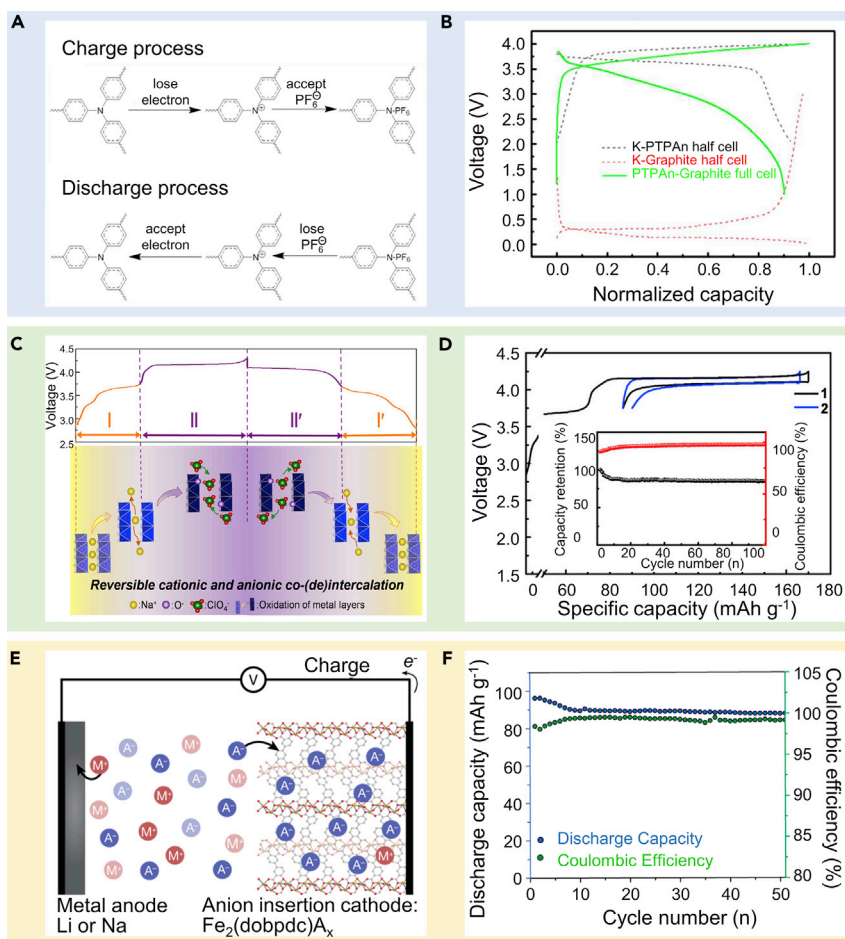


Figure 9. Insertion-type DIBs based on non-graphite-based cathodes and non-aqueous electrolytes

(A and B) Shown are the (A) mechanism of the PTPAn molecule accepting anions during charging and losing anions during discharging and the (B) typical charge-discharge curves of a graphite || PTPAn full cell, and the corresponding two half cells (K metal||PTPAn and K metal||graphite), Reprinted with permission from Fan et al.⁹² Copyright 2017 American Chemical Society.

(C and D) Shown are the (C) typical charge-discharge profiles of the DIB based on $\text{Na}_{0.5}\text{Ni}_{0.25}\text{Mn}_{0.75}\text{O}_2$ cathode (top), and the schematic illustration showing the reversible anion intercalation-deintercalation process in such cathode (bottom) and the (D) charge-discharge curves of such DIB in the initial two cycles at 20 mA g^{-1} , and the corresponding cycling performance (inset), Reprinted with permission from Li et al.⁸⁷ Copyright 2018 Elsevier.

(E and F) Shown are the (E) schematic illustration showing the working mechanism of the DIB with a $\text{Fe}_2(\text{dobpdc})\text{A}_x$ MOF cathode and the (F) cycling performance of the Na metal|| $\text{Fe}_2(\text{dobpdc})\text{A}_x$ cell at 1 C. Reproduced with permission from Aubrey et al.⁸⁸ Copyright 2015 American Chemical Society.

cathode materials need to be elucidated via *in situ* characterization techniques for the development of novel and effective cathode materials.

Aqueous insertion-type DIBs

Up to now, most insertion-type DIBs have operated in organic electrolytes, in which highly flammable solvents (e.g., EC and EMC) introduce safety concerns, such as fire and explosion risks. In this regard, applying aqueous electrolytes for insertion-type DIBs can greatly enhance battery safety.^{94,95} Besides this aspect, using aqueous electrolytes can further reduce the cost of insertion-type DIBs, which can better meet the needs of large-scale energy storage.^{26,96}

Based on their anion characteristics, aqueous insertion-type DIBs can be divided into simple anion-based types (e.g., NO_3^-) and superhalide-based types (e.g., $[\text{ZnCl}_x]^{2-x}$ and $[\text{MgCl}_x]^{2-x}$). Jiang et al. reported an aqueous DIB employing Mn_3O_4 as the cathode, activated carbon as the anode, and 1 m NH_4NO_3 aqueous solution as the electrolyte.¹⁸ The NO_3^- anions are reversibly intercalated or de-intercalated into/from the cathode material. The as-developed aqueous DIB delivered fast reaction kinetics and high cycling stability. At a current density of 1 A g⁻¹, the cell delivered 50 mA h g⁻¹ after 3,500 cycles with 99% Coulombic efficiency based on the mass of Mn_3O_4 cathode. Electrochemical quartz crystal microbalance tests revealed that the Mn_3O_4 cathode experienced a mass gain during the charge process of 92 g mol⁻¹ e⁻¹, suggesting that two water molecules were co-inserted into Mn_3O_4 whenever one NO_3^- anion inserted. Furthermore, Fourier-transformed Mn K-edge extended X-ray absorption fine structure spectroscopy (EXAFS) spectra indicated that the insertion of NO_3^- changed the long-range order and the amorphous sites of Mn_3O_4 in the pristine electrode and formed a hybrid matrix comprising both crystalline and amorphous nanodomains.

It is well-known that the narrow electrochemical stability window of dilute aqueous electrolytes (i.e., 1.23 V) greatly limits the energy density of aqueous batteries. Highly concentrated electrolytes have been developed to expand the electrochemical stability window of aqueous electrolytes, and thus enable the applications of energy-density electrochemical redox couples. Recently, Guo et al. reported a new cathode material based on nitrogen-doped microcrystalline graphene-like carbon, and coupled this with highly concentrated (30 m) ZnCl_2 electrolytes in Zn-based DIBs.⁹⁷ The unique carbon structure of the cathode material enabled the $[\text{ZnCl}_x]^{2-x}$ anions to be reversibly adsorbed and inserted via the electrical double layer. When paired with a Zn metal anode, this aqueous superhalide-based system exhibited a high-potential plateau at 1.85 V, and the cell delivered a high capacity of 134 mA h g⁻¹ based on the cathode material mass. A reversible insertion of Mg-Cl superhalides into graphite was realized in an aqueous deep eutectic solvent (DES) composed of 9 m magnesium chloride (MgCl_2) and 30 m choline chloride (ChCl).²⁶ The as-developed activated carbon||graphite cell achieved a high initial reversible capacity of 150 mA h g⁻¹ based on the mass of graphite cathode with a long cycle life of >300 cycles at 100 mA g⁻¹. This initial reversible capacity is significantly larger than that of reversible oxidative anion insertion in graphite reported previously. In most cases, the insertion of large complex anions causes dramatic structural transformation of the graphite electrodes. Interestingly, the *ex situ* XRD of the graphite electrode confirmed the absence of the (002) peak shifting corresponding to the formation of staged graphite intercalation compounds. This suggested that the operating mechanism of aqueous superhalide-based DIBs was significantly different from that of traditional organic electrolyte-based DIBs, where the insertion of Mg-Cl superhalides transformed graphite into partially turbostratic rather than staged graphite intercalation compounds. The operating mechanisms of such new shuttle carriers should be further investigated for the future development of aqueous DIBs. Overall, expanding the electrochemical stability window of aqueous electrolytes and developing high-energy electrode couples based on novel redox chemistry remains a promising area for future aqueous insertion-type DIBs.

CONVERSION-TYPE AND INSERTION-CONVERSION DIBs

Generally, if the battery operation voltage is higher than the anion's oxidation potential, the anions will undergo a redox reaction at the cathode. Conversion-type DIBs have been established based on such reversible anion redox couples. Typical

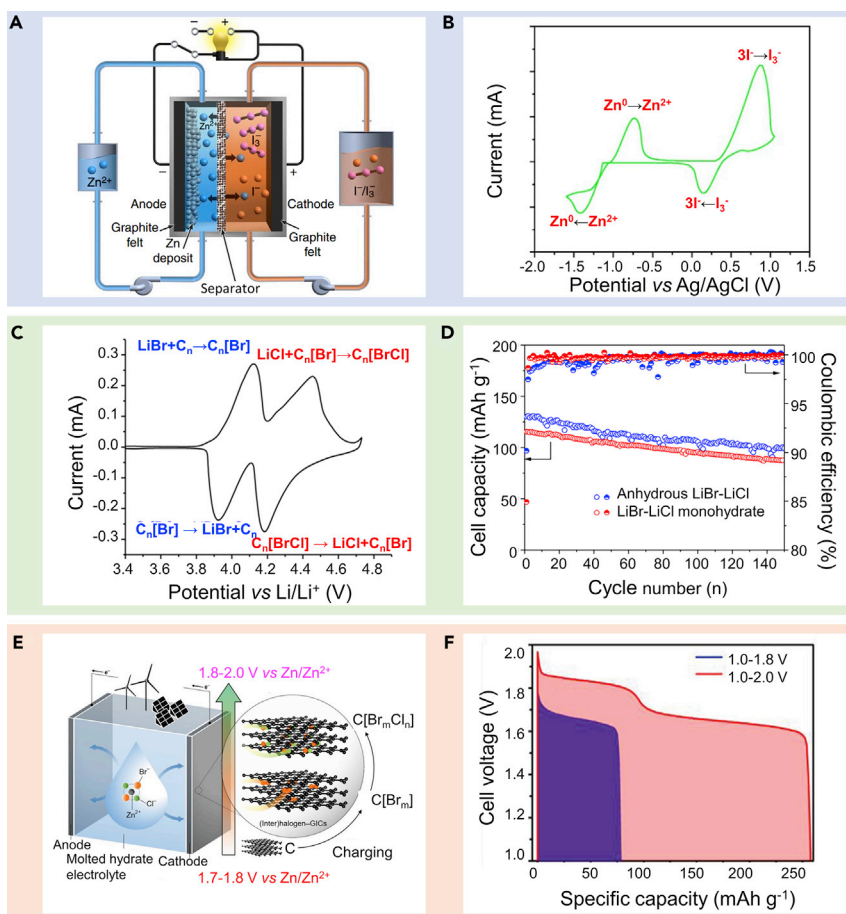


Figure 10. Conversion-type and conversion-insertion-type DIBs

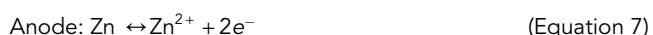
(A and B) Shown are the (A) schematic representation of the zinc-polyiodide flow battery and the (B) CV of a glassy carbon electrode in a 0.085 M ZnI₂ electrolyte on at the scan rate of 50 mV s⁻¹.

Reprinted with permission from Li et al.²⁴ Copyright 2015 Nature Publishing Group.

(C and D) Shown are the (C) CV of the LBC-G cathode at a scan rate of 0.05 mV s⁻¹ and the (D) cycling performance of graphite||LBC-G full cell at 0.2 C. Reprinted with permission from Yang et al.¹⁹ Copyright 2019 Nature Publishing Group.

(E and F) Shown are the (E) schematic representation of a Zn-based conversion-insertion-type DIB using a molten hydrate electrolyte and the (F) comparison of the discharge profiles involving single-halogen (dark blue) or dual-halogen (pink) redox couples. Reprinted with permission from Liu et al.⁹⁹ Copyright 2020 Wiley-VCH.

examples of conversion-type DIBs include zinc-bromine batteries⁹⁸ and zinc-iodine batteries.²⁴ Li et al. reported a conversion-type zinc-iodine DIB based on flow-battery configuration.²⁴ As shown in Figure 10A, in such a system, the cathode and anode experience reactions as follows:



These reactions can be clearly identified from the corresponding peaks in the CV curves, as shown in Figure 10B. Zinc-iodine batteries with a 3.5 M ZnI₂ aqueous electrolyte delivered a respectable specific discharge capacity of 125 A h L⁻¹ (based on the volume of catholyte) at 10 mA cm⁻², and the early capacity was retained well during 40 cycles.

As mentioned above, as a redox-amphoteric host material, graphite can not only be employed as a donor-type anode for cation intercalation but can also be applied as an acceptor-type cathode for anion intercalation. Although the graphite cathodes exhibit high operating voltage in DIBs, their specific capacity is generally less than 150 mA h g^{-1} .²⁵ Accordingly, Yang et al. developed a novel conversion-insertion-type DIB to further increase the capacity of graphite cathode.¹⁹ The as-developed DIB consisted of a $(\text{LiBr})_{0.5}(\text{LiCl})_{0.5}$ -graphite (LBC-G) cathode prepared by mixing anhydrous lithium bromide (LiBr) and lithium chloride (LiCl) with graphite powder, a graphite anode protected by a highly fluorinated ether (HFE) polymer gel, and a 21 m LiTFSI + 7 m lithium trifluoromethanesulfonate (LiOTf) “water-in-bisalt (WIBS)” aqueous-gel electrolyte. The operating mechanism of the cathode involved a two-step redox reaction. When charged to 4.2 V, bromide ions (Br^-) were first oxidized to elemental bromine (Br^0), and then intercalated into graphite to form a $\text{C}_n[\text{Br}]$ compound. When the cell was further charged to 4.5 V, chloride ions (Cl^-) were oxidized to a near-zero state (Cl^0) and subsequently intercalated into graphite to form a mixed intercalation compound $\text{C}_n[\text{BrCl}]$. This redox reaction was accompanied by the release of Li-ions into the aqueous gel electrolyte, and there takes place the intercalation of Li-ions into the graphite anode. The corresponding CV curve of the LBC-G cathode displayed two distinct plateaus attributing to the two-step redox reaction and demonstrated that the cathode redox reaction was highly reversible (Figure 10C). The LBC-G cathode delivered a high reversible capacity of 243 mA h g^{-1} with a Coulombic efficiency of 99.8%, and the constructed graphite||LBC-G full cell exhibited a high energy density of 460 Wh kg^{-1} (based on the total mass of cathode and anode) with good cycling stability (Figure 10D). The energy density of the aqueous conversion-insertion-type DIB was slightly larger than that of state-of-the-art non-aqueous Li-ion batteries, showing the attractive potential for practical applications.

Such a conversion-insertion mechanism has also been extended to multivalent-ion batteries (e.g., Zn-based batteries). Recently, Liu reported a Zn-based conversion-insertion-type DIB containing a graphite cathode, a $\text{ZnCl}_2 \cdot 0.03\text{KBr} \cdot 2\text{H}_2\text{O}$ molten hydrate electrolyte, and a Zn metal anode.⁹⁹ As shown in Figure 10E, the two-step redox reaction of the cathode was similar to that in Li-based conversion-insertion-type DIBs in which the formation of $\text{C}[\text{Br}_m]$ was indispensable for the subsequent intercalation of Cl^0 into graphite. The utilization of dual-halogen redox couples (i.e., Br^0/Br^- and Cl^0/Cl^-) effectively increased the average discharge voltage from 1.60 V (Br^0/Br^- solely) to 1.71 V and improved the capacity from 78 to 257 mA h g^{-1} based on the total mass of cathode materials (Figure 10F), which is quite promising compared with aqueous Zn-ion batteries with low operating voltages ($<1 \text{ V}$) or Zn-based DIBs with limited capacity values ($<120 \text{ mA h g}^{-1}$). The as-developed full cell exhibited a cycle life over 100 cycles. Future work on conversion-insertion-type DIBs needs to focus on the simplification of current complicated battery configurations and realizing the conversion-intercalation chemistry in non-aqueous electrolytes with low salt concentrations and viscosity.

RDIBs

RDIBs share similar working principles with DIBs, whereas the types of ions their electrodes host are totally the opposite. Moreover, during the charging process, ions move from electrolyte to electrodes in DIBs; but in RDIBs, they are released from electrodes into the electrolyte. Up until now, the RDIB chemistry has been only realized in the presence of aqueous electrolytes. Wu et al. reported such a RDIB chemistry based on a highly concentrated (30 m) ZnCl_2 aqueous electrolyte.²⁰ In

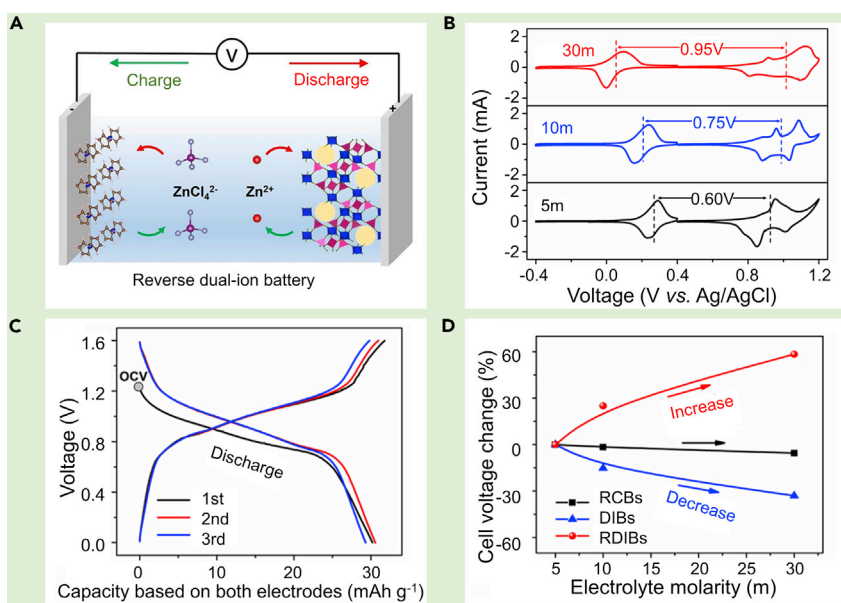


Figure 11. RDIBs

(A–D) Shown are the (A) schematic illustration of a Zn-based RDIB, (B) CV curves of such RDIB with electrolytes with different salt concentrations at 1 mV s⁻¹, (C) charge-discharge profiles of the RDIB full cell at 1 C rate (1 C = 30 mA g⁻¹ based on the total mass of Zn₃[Fe(CN)₆]₂ cathode and ferrocene/carbon composite anode), and (D) voltage changes of full cells in ZnCl₂ electrolytes with different salt concentrations: rocking-chair batteries (RCBs), DIBs, and RDIBs. Reprinted with permission from Wu et al.²⁰ Copyright 2019 American Chemical Society.

this Zn-based RDIB, upon discharge, Zn²⁺ cations were inserted into a Zn₃[Fe(CN)₆]₂ cathode, meanwhile ZnCl₄²⁻ anions were inserted into a ferrocene anode (Figure 11A). Conversely, the Zn²⁺ cations and ZnCl₄²⁻ anions were de-intercalated from the electrodes simultaneously during the charge process. The ion-insertion potentials were altered in the high concentrated aqueous electrolyte, i.e., the cation-insertion potential was increased, whereas the anion-insertion potential was lowered. The application of such a highly concentrated aqueous electrolyte reduced the availability of free water molecules and, hence, widened the electrolyte electrochemical window. As a result, the battery operation voltage was enlarged by 0.35 V compared to that of the 5 M aqueous electrolyte (Figure 11B). This effect largely improved the energy density of the RDIBs. Such a full cell delivered a specific energy density of 21.0 Wh kg⁻¹ with a reversible capacity of 30 mA h g⁻¹ based on the mass of both electrode materials and electrolyte (Figure 11C). Interestingly, the voltage of RDIBs is consistently increased with increasing the electrolyte concentration, while the reverse phenomenon occurs in DIBs, further demonstrating the application merits of highly concentrated aqueous electrolytes in RDIBs (Figure 11D). Zhang et al. reported a RDIB system based on F⁻ cations and Na⁺ anions as charge carriers, with BiF₃ applied as anode, sodium manganese oxide (Na_{0.44}MnO₂) as cathode, and NaF aqueous solution as the electrolyte.¹⁰⁰ These batteries function from an initial charging process, in which F⁻ ions are released from a BiF₃ anode to form bismuth metal. Meanwhile, Na⁺ ions are de-inserted from a Na_{0.44}MnO₂ cathode to form Na_{0.44-x}MnO₂. The electrode reactions are highly reversible and deliver a discharge capacity of \approx 92.6 mA h g⁻¹ at 100 mA g⁻¹ based on the mass of BiF₃. The battery configuration of RDIBs should prompt the future development of cation-deficient and metal-anode-free electrode materials for low-cost energy storage.

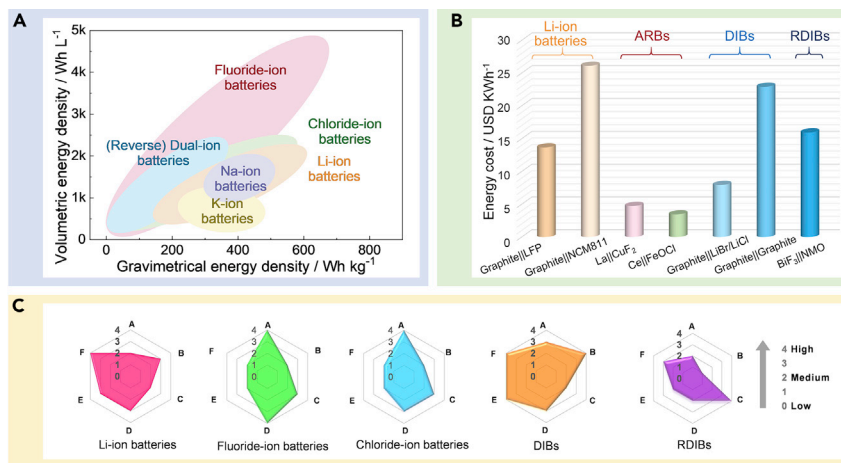


Figure 12. Comparisons of various battery chemistries

(A) Comparison of theoretical volumetric and gravimetric energy density of different battery technologies. The theoretical energy densities are calculated based on the total mass of anode and cathode active materials. For DIBs and RDIBs, the mass of salt involved the electrochemical process has been taken into account.

(B) Cost analysis of different battery systems based on the cost of the electrode materials. For DIBs and RDIBs, the mass of salt involved the electrochemical process has been taken into account.

(C) Radar diagrams of various batteries based on six parameters. (A, low cost; B, voltage; C, safety; D, volumetric energy density; E, lifespan; F, rate performance).

CONCLUSIONS AND PROSPECT

ASBs possess inherently different characteristics compared with conventional metal-ion batteries (e.g., Li-ion batteries), as anions serve as charge carriers shuttling between electrodes. In recent years, three types of ASBs (i.e., ARBs, DIBs [including insertion-type, conversion-type, and conversion-insertion-type], and RDIBs) have received tremendous attention and gained regard as promising technologies for large-scale energy storage. Figure 12A compares the theoretical energy densities (see Tables S2 and S3 for details) of representative ASBs (i.e., fluoride-ion batteries, chloride-ion batteries, insertion-type DIBs, conversion-type DIBs, conversion-insertion-type DIBs, and RDIBs) and metal-ion batteries (i.e., Li-ion batteries, Na-ion batteries, and K-ion batteries).^{19,29,41,61} It is clearly seen that ARBs promise significantly higher theoretical energy densities than metal-ion batteries, especially in terms of volumetric energy density.^{19,22} Figure 12B illustrates a cost analysis of different battery systems based on the cost of their electrode materials (see Tables S4 and S5 for details). It is clearly seen that ASBs deliver obvious low-cost advantages compared with existing commercial Li-ion batteries (e.g., graphite||LiFePO₄ (LFP), graphite||LiNi_{0.8}Mn_{0.1}Co_{0.1}O₂ (NCM₈₁₁)) because of the large availability and low cost of raw materials. Furthermore, in Figure 12C we have summarized the characteristics of different ASBs from six different aspects, including cost, operating voltage, safety, volumetric energy density, lifespan, and rate performance. We note that ARBs possess high volumetric energy density with extremely low cost, whereas DIBs have the merit of high output voltages and relatively good rate performance, and RDIBs exhibit high safety. Up to now, the general challenges for ASBs are unsatisfactory reversibility, limited lifespan, and sluggish reaction kinetics. Although certain progress has been made on improving the performances of ASBs in recent years, great efforts are still needed in the following areas:

- (1) ARBs possess the advantages of high theoretical energy and low cost. However, because of the relatively large radii of anions, the repeated insertion or

de-insertion of anions into hosts usually results in huge electrode volumetric changes. These trigger severe pulverization and decomposition of host materials and aggravate the side reactions between electrodes and electrolytes, leading to short cycling life. Therefore, it is important to develop high-performance electrode materials to boost the performance of ARBs. Stable layered-structure materials (e.g., LDHs) could endow fast kinetics of reversible anion insertion or de-insertion processes. Hence, they are expected as promising electrode materials for ARBs. Moreover, it is also essential to develop advanced electrolytes with high room-temperature ionic conductivity, electrochemical stability, and electrode compatibility for high-performance ARBs.

- (2) For DIBs, although the high working voltage ranges benefit the improvement of battery energy density. Whereas, such high output voltages also cause severe electrolyte decomposition and safety hazards (i.e., thermal runaway). Therefore, it necessitates developing high-voltage electrolytes with non-flammability and high interfacial compatibility for DIBs. In this regard, quasi-solid-state electrolytes are expected as feasible options in the future development of DIBs. Moreover, considering elemental metals is generally applied as anode materials for DIBs, establishing stable anode|electrolyte interfaces by constructing a robust artificial SEI layer²⁷ or optimizing electrolyte constitution²³ is crucial to suppress the metallic dendrite growth and side reactions between anodes and electrolytes, thus improving the cycling life and safety of batteries.
- (3) The RDIB chemistry has only been realized in aqueous electrolytes, and only a few kinds of electrode materials have been reported. The output voltages of existing RDIBs are relatively low, which gives rise to limited battery energy densities. Therefore, it is critical to increase the battery output voltage via screening electrode couples (i.e., cathode materials with relatively high cation-insertion-voltage and anode materials with relatively low anion-accommodating-voltage) together with developing compatible electrolytes for the development of RDIBs in the future.
- (4) In ASBs, microscopic mechanisms of electrochemical reactions need to be further clarified. These include the solvation or de-solvation processes of inserted anions associated with interfacial ionic transport and mass change behaviors, the characteristics and compositions of SEI and CEI layers, the electrode/electrolyte structural evolution, and the interfacial side reactions during cycling. Thus, more advanced characterization technologies, such as *in operando* characterization methods (e.g., *in situ* XPS and *in situ* transmission electron microscope [TEM]), time of flight secondary ion mass spectrometry (TOF-SIMS), and electrochemical quartz crystal microbalance analysis, should be experimentally employed to deepen the current understanding of ASB chemistries.
- (5) The previous research on ASBs tended to evaluate electrode performance based on single electrodes of small areas, which cannot fully reflect their performance in practical applications. Therefore, large-area soft-packaged batteries need to be developed to better evaluate the practical-application potential of ASBs.

As an emerging low-cost energy storage technology, the development of ASBs is still in a relatively young stage. Unremitting efforts focusing on the above issues will promote the development of new electrode host materials, tailored electrolytes, and optimized cell configurations, which can endow ASBs with more competitive features over metal-ion batteries. Furthermore, research on ASBs can expand the selection pool of chemistries, charge carriers, and energy storage materials for next-generation batteries.

SUPPLEMENTAL INFORMATION

Supplemental information can be found online at <https://doi.org/10.1016/j.chempr.2021.02.004>.

ACKNOWLEDGMENTS

B.L. would like to acknowledge the support by National Nature Science Foundation of China (51872157 and 52072208), Shenzhen Technical Plan Project (JCYJ20170412170911187 and JCYJ20170817161753629), Special Fund Project for Strategic Emerging Industry Development of Shenzhen (20170428145209110), Guangdong Technical Plan Project (2017B090907005), and Local Innovative and Research Teams Project of Guangdong Pearl River Talents Program (2017BT01N111). Devices Testing Center in Tsinghua Shenzhen International Graduate School was also gratefully acknowledged. G.W. would like to acknowledge the support by the Australian Research Council (ARC) Discovery projects (DP170100436, DP180102297, and DP200101249). X.J. is grateful for the financial support from U.S. National Science Foundation awards DMR-2004636 and CBET-1551693.

AUTHOR CONTRIBUTIONS

Q.L., Y.W., and D.Z. conducted the literature search; all authors wrote, discussed, and revised the manuscript.

DECLARATION OF INTERESTS

The authors declare no competing interests.

REFERENCES

1. Armand, M., and Tarascon, J.M. (2008). Building better batteries. *Nature* **451**, 652–657.
2. Wang, Y.Z., Zhou, D., Palomares, V., Shanmukaraj, D., Sun, B., Tang, X., Wang, C.S., Armand, M., Rojo, T., and Wang, G. (2020). Revitalising sodium-sulfur batteries for non-high-temperature operation: a crucial review. *Energy Environ. Sci.* **13**, 3848–3879, <https://doi.org/10.1039/DOEE02203A>.
3. Armand, M. (1980). Intercalation electrodes. In *Materials for Advanced Batteries*, D.W. Murphy, J. Broadhead, and B.C.H. Steele, eds. (Plenum Press), pp. 145–146.
4. Wang, S., Yu, Z.J., Tu, J., Wang, J.X., Tian, D.H., Liu, Y.J., and Jiao, S.Q. (2016). A novel aluminum-ion battery: $\text{Al}/\text{AlCl}_3[\text{EMIm}]\text{Cl}/\text{Ni}_3\text{S}_2$ @graphene. *Adv. Energy Mater.* **6**, 1600137.
5. Wang, S., Jiao, S., Tian, D., Chen, H.S., Jiao, H., Tu, J., Liu, Y., and Fang, D.N. (2017). A novel ultrafast rechargeable multi-ions battery. *Adv. Mater.* **29**, 1606349–1606356.
6. Rudorff, F.W., and Hofman, U. (1938). Über graphitsalze. *Zeitschrift für anorganische und allgemeine chemie* **238**, 1–50.
7. Panero, S., Spila, E., and Scrosati, B. (1996). A new type of a rocking-chair battery family based on a graphite anode and a polymer cathode. *J. Electrochem. Soc.* **143**, L29–L30.
8. Seel, A.J., and Dahn, R.D. (2000). Electrochemical intercalation of PF_6^- into graphite. *J. Electrochem. Soc.* **147**, 892–898.
9. Anji Reddy, M.A., and Fichtner, M. (2011). Batteries based on fluoride shuttle. *J. Mater. Chem.* **21**, 17059–17063.
10. Zhao, X., Ren, S., Bruns, M., and Fichtner, M. (2014). Chloride ion battery: a new member in the rechargeable battery family. *J. Power Sources* **245**, 706–711.
11. Liang, G.J., Mo, F.N., Ji, X.L., and Zhi, C.Y. (2020). Non-metallic charge carriers for aqueous batteries. *Nat. Rev. Mater.* **6** (109–123), <https://doi.org/10.1038/s41578-020-00241-4>.
12. Zabel, H., Solin, S.A., and Hwan, D.M. (1990). *Graphite Intercalation Compounds I: Structure and Dynamics* (Springer).
13. Hou, X., Zhang, Z., Shen, K., Cheng, S., He, Q., Shi, Y., Yu, D.Y.W., Su, C., Li, L., and Chen, F. (2019). An aqueous rechargeable fluoride ion battery with dual fluoride electrodes. *J. Electrochem. Soc.* **166**, A2419–A2424.
14. Chen, F., Leong, Z.Y., and Yang, H.Y. (2017). An aqueous rechargeable chloride ion battery. *Energy Storage Mater.* **7**, 189–194.
15. McCullough, F.P., Levine, C.A., and Snelgrove, R.V. (1989). Secondary battery (U.S. Patent US 4830938), filed March 17, 1988, and published.
16. Richard, T., Hugh, C., Joan, F., and Paul, C. (1994). Dual intercalating molten electrolyte batteries. *J. Electrochem. Soc.* **141**, L73–L76.
17. Placke, T., Fromm, O., Lux, S.F., Bieker, P., Rothermel, S., Meyer, H., Passerini, S., and Winter, M. (2012). Reversible intercalation of bis(trifluoromethanesulfonyl)imide anions from an ionic liquid electrolyte into graphite for high performance dual-ion cells. *J. Electrochem. Soc.* **159**, A1755–A1765.
18. Jiang, H., Wei, Z., Ma, L., Yuan, Y., Hong, J.J., Wu, X., Leonard, D.P., Holoubek, J., Razink, J.J., Stickle, W.F., et al. (2019). An aqueous dual-ion battery cathode of Mn_3O_4 via reversible insertion of nitrate. *Angew. Chem. Int. Ed. Engl.* **58**, 5286–5291.
19. Yang, C., Chen, J., Ji, X., Pollard, T.P., Lü, X., Sun, C.J., Hou, S., Liu, Q., Liu, C., Qing, T., et al. (2019). Aqueous Li-ion battery enabled by halogen conversion-intercalation chemistry in graphite. *Nature* **569**, 245–250.
20. Wu, X., Xu, Y., Zhang, C., Leonard, D.P., Markir, A., Lu, J., and Ji, X. (2019). Reverse dual-ion battery via a ZnCl_2 water-in-salt electrolyte. *J. Am. Chem. Soc.* **141**, 6338–6344.
21. Zhao, X., Zhao-Karger, Z., Fichtner, M., and Shen, X. (2020). Halide-based materials and chemistry for rechargeable batteries. *Angew. Chem. Int. Ed. Engl.* **59**, 5902–5949.
22. Placke, T., Heckmann, A., Schmuck, R., Meister, P., Beltrop, K., and Winter, M. (2018). Perspective on performance, cost, and technical challenges for practical dual-ion batteries. *Joule* **2**, 2528–2550.
23. Xu, X., Lin, K., Zhou, D., Liu, Q., Qin, X., Wang, S., He, S., Kang, F., Li, B., and Wang, G. (2020). Quasi-solid-state dual-ion sodium metal batteries for low-cost energy storage. *Chem* **6**, 902–918.

24. Li, B., Nie, Z., Vijayakumar, M., Li, G., Liu, J., Sprengle, V., and Wang, W. (2015). Ambipolar zinc-polyiodide electrolyte for a high-energy density aqueous redox flow battery. *Nat. Commun.* 6, 6303.

25. Placke, T., and Winter, M. (2019). Boosting aqueous batteries by conversion-intercalation graphite cathode chemistry. *Joule* 3, 1184–1187.

26. Martin, A., Kiarie, W., Chang, B., and Thuo, M. (2020). Cover picture: chameleon metals: autonomous nano-texturing and composition inversion on liquid metals surfaces. *Angew. Chem. Int. Ed. Engl.* 59, 1.

27. Hao, J., Li, X., Song, X., and Guo, Z. (2019). Recent progress and perspectives on dual-ion batteries. *EnergyChem* 1, 100004, <https://doi.org/10.1016/j.enchem.2019.100004>.

28. Patro, L.N., and Hariharan, K. (2013). Fast fluoride ion conducting materials in solid state ionics: an overview. *Solid State Ionics* 239, 41–49.

29. Thieu, D.T., Fawey, M.H., Bhatia, H., Diermant, T., Chakravadhanula, V.S.K., Behm, R.J., Kübel, C., and Fichtner, M. (2017). CuF₂ as reversible cathode for fluoride ion batteries. *Adv. Funct. Mater.* 27, 1701051.

30. Nowroozi, M.A., Ivlev, S., Rohrer, J., and Clemens, O. (2018). La₂CoO₄: a new intercalation based cathode material for fluoride ion batteries with improved cycling stability. *J. Mater. Chem. A* 6, 4658–4669.

31. Nowroozi, M.A., Wissel, K., Rohrer, J., Munnangi, A.R., and Clemens, O. (2017). LaSrMnO₄: reversible electrochemical intercalation of fluoride ions in the context of fluoride ion batteries. *Chem. Mater.* 29, 3441–3453.

32. Mohammad, I., Chable, J., Witter, R., Fichtner, M., and Reddy, M.A. (2018). Synthesis of fast fluoride-ion-conductive fluorite-type Ba_{1-x}Sb_xF_{2+x} (0.1 ≤ x ≤ 0.4): a potential solid electrolyte for fluoride-ion batteries. *ACS Appl. Mater. Interfaces* 10, 17249–17256.

33. Rongeat, C., Reddy, M.A., Witter, R., and Fichtner, M. (2013). Nanostructured fluorite-type fluorides as electrolytes for fluoride ion batteries. *J. Phys. Chem. C* 117, 4943–4950.

34. Zhang, L., Anji Reddy, M., and Fichtner, M. (2015). Development of tsynite-type fluoride conducting thin film electrolytes for fluoride ion batteries. *Solid State Ionics* 272, 39–44.

35. Bhatia, H., Thieu, D.T., Pohl, A.H., Chakravadhanula, V.S.K., Fawey, M.H., Kübel, C., and Fichtner, M. (2017). Conductivity optimization of tsynite-type La_{1-x}Ba_xF_{3-x} solid electrolytes for advanced fluoride ion battery. *ACS Appl. Mater. Interfaces* 9, 23707–23715.

36. Mohammad, I., Witter, R., Fichtner, M., and Anji Reddy, M. (2018). Room-temperature, rechargeable solid-state fluoride-ion batteries. *ACS Appl. Energy Mater.* 1, 4766–4775.

37. Okazaki, K., Uchimoto, Y., Abe, T., and Ogumi, Z. (2017). Charge-discharge behavior of bismuth in a liquid electrolyte for rechargeable batteries based on a fluoride shuttle. *ACS Energy Lett.* 2, 1460–1464.

38. Davis, V.K., Bates, C.M., Omichi, K., Savoie, B.M., Momčilović, N., Xu, Q., Wolf, W.J., Webb, M.A., Billings, K.J., Chou, N.H., et al. (2018). Room-temperature cycling of metal fluoride electrodes: liquid electrolytes for high-energy fluoride ion cells. *Science* 362, 1144–1148.

39. Gschwind, F., Zao-Karger, Z., and Fichtner, M. (2014). A fluoride-doped PEG matrix as an electrolyte for anion transportation in a room-temperature fluoride ion battery. *J. Mater. Chem. A* 2, 1214–1218.

40. Yin, Q., Rao, D., Zhang, G., Zhao, Y., Han, J., Lin, K., Zheng, L., Zhang, J., Zhou, J., and Wei, M. (2019). CoFe-Cl layered double hydroxide: a new cathode material for high-performance chloride ion batteries. *Adv. Funct. Mater.* 29, 1900983.

41. Zhao, X., Zhao-Karger, Z., Wang, D., and Fichtner, M. (2013). Metal oxychlorides as cathode materials for chloride ion batteries. *Angew. Chem. Int. Ed. Engl.* 52, 13621–13624.

42. Gao, P., Reddy, M.A., Mu, X., Diermant, T., Zhang, L., Zhao-Karger, Z., Chakravadhanula, V.S., Clemens, O., Behm, R.J., and Fichtner, M. (2016). VOCl as a cathode for rechargeable chloride ion batteries. *Angew. Chem. Int. Ed. Engl.* 55, 4285–4290.

43. Yu, T., Li, Q., Zhao, X., Xia, H., Ma, L., Wang, J., Meng, Y.S., and Shen, X. (2017). Nanoconfined iron oxychloride material as a high-performance cathode for rechargeable chloride ion batteries. *ACS Energy Lett.* 2, 2341–2348.

44. Zhao, X., Zhao, Z., Yang, M., Xia, H., Yu, T., and Shen, X. (2017). Developing polymer cathode material for the chloride ion battery. *ACS Appl. Mater. Interfaces* 9, 2535–2540.

45. Gschwind, F., Steinle, D., Sandbeck, D., Schmidt, C., and von Hauff, E. (2016). Facile preparation of chloride-conducting membranes: first step towards a room-temperature solid-state chloride-ion battery. *ChemistryOpen* 5, 525–530.

46. Chen, C., Yu, T., Yang, M., Zhao, X., and Shen, X. (2019). An all-solid-state rechargeable chloride ion battery. *Adv Sci (Weinh)* 6, 1802130.

47. Xia, T., Li, Y., Huang, L., Ji, W., Yang, M., and Zhao, X. (2020). Room-temperature stable inorganic halide perovskite as potential solid electrolyte for chloride ion batteries. *ACS Appl. Mater. Interfaces* 12, 18634–18641.

48. Gao, P., Zhao, X., Zhao-Karger, Z., Diermant, T., Behm, R.J., and Fichtner, M. (2014). Vanadium oxychloride/magnesium electrode systems for chloride ion batteries. *ACS Appl. Mater. Interfaces* 6, 22430–22435.

49. Zhao, X., Li, Q., Zhao-Karger, Z., Gao, P., Fink, K., Shen, X., and Fichtner, M. (2014). Magnesium anode for chloride ion batteries. *ACS Appl. Mater. Interfaces* 6, 10997–11000.

50. Yin, Q., Zhang, J., Luo, J., Han, J., Shao, M., and Wei, M. (2020). A new family of rechargeable batteries based on halide ions shuttling. *Chem. Eng. J.* 389, 124376.

51. Lin, M.C., Gong, M., Lu, B., Wu, Y., Wang, D.Y., Guan, M., Angell, M., Chen, C., Yang, J., Hwang, B.J., and Dai, H. (2015). An ultrafast rechargeable aluminium-ion battery. *Nature* 520, 325–328.

52. Wang, D.-Y., Wei, C.-Y., Lin, M.-C., Pan, C.-J., Chou, H.L., Chen, H.-A., Gong, M., Wu, Y., Yuan, C., Angell, M., et al. (2017). Advanced rechargeable aluminium ion battery with a high-quality natural graphite cathode. *Nat. Commun.* 8, 14283.

53. Yu, Z., Jiao, S., Tu, J., Song, W., Lei, H., Jiao, H., Chen, H.A., and Fang, D. (2019). Gel electrolytes with a wide potential window for high-rate Al-ion batteries. *J. Mater. Chem. A* 7, 20348–20356.

54. Suo, L.M., Borodin, O., Gao, T., Olguin, M., Ho, J., Fan, X.L., Luo, C., Wang, C.S., and Xu, K. (2015). "Water-in-salt" electrolyte enables high-voltage aqueous lithium-ion chemistries. *Science* 350, 938–943.

55. Ling, T., Da, P.F., Zheng, X.L., Ge, B.H., Hu, Z.P., Wu, M.Y., Du, X.W., Hu, W.B., Jaroniec, M., and Qiao, S.Z. (2018). Atomic-level structure engineering of metal oxides for high-rate oxygen intercalation pseudocapacitance. *Sci. Adv.* 4, eaau6261.

56. Parker, J.F., Chervin, C.N., Pala, I.R., Machler, M., Burz, M.F., Long, J.W., and Rolison, D.R. (2017). Rechargeable nickel-3D zinc batteries: an energy-dense, safer alternative to lithium-ion. *Science* 356, 415–418.

57. Huang, Z.D., Li, X.L., Yang, Q., Ma, L.T., Mo, F.N., Liang, G.J., Wang, D.H., Liu, Z.X., Li, H.F., and Zhi, C.Y. (2019). Ni₃S₂/Ni nanosheet arrays for high-performance flexible zinc hybrid batteries with evident two-stage charge and discharge processes. *J. Mater. Chem. A* 7, 18915–18924.

58. Ji, X.L. (2019). A paradigm of storage batteries. *Energy Environ. Sci.* 12, 3203–3224.

59. Liang, G.J., Mo, F.N., Wang, D.H., Li, X.L., Huang, Z.D., Li, H.F., and Zhi, C.Y. (2020). Commencing mild Ag-Zn batteries with long-term stability and ultra-flat voltage platform. *Energy Storage Mater* 25, 86–92.

60. Hu, X., Chen, F., Wang, S., Ru, Q., Chu, B., Wei, C., Shi, Y., Ye, Z., Chu, Y., Hou, X., and Sun, L. (2019). Electrochemical performance of Sb₄O₅Cl₂ as a new anode material in aqueous chloride-ion battery. *ACS Appl. Mater. Interfaces* 11, 9144–9148.

61. Zhou, X., Liu, Q., Jiang, C., Ji, B., Ji, X., Tang, Y., and Cheng, H.M. (2020). Strategies towards low-cost dual-ion batteries with high performance. *Angew. Chem. Int. Ed. Engl.* 59, 3802–3832.

62. Bellani, S., Wang, F., Longoni, G., Najafi, L., Oropesa-Nuñez, R., Del Rio Castillo, A.E., Prato, M., Zhuang, X., Pellegrini, V., Feng, X., and Bonaccorso, F. (2018). WS₂-graphite dual-ion batteries. *Nano Lett.* 18, 7155–7164.

63. Rothermel, S., Meister, P., Schmuelling, G., Fromm, O., Meyer, H.-W., Nowak, S., Winter, M., and Placke, T. (2014). Dual-graphite cells based on the reversible intercalation of bis(trifluoromethanesulfonyl)imide anions from an ionic liquid electrolyte. *Energy Environ. Sci.* 7, 3412–3423.

64. Xiang, L., Ou, X., Wang, X., Zhou, Z., Li, X., and Tang, Y. (2020). Highly concentrated electrolyte towards enhanced energy density

and cycling life of dual-ion battery. *Angew. Chem. Int. Ed. Engl.* 59, 17924–17930.

65. Read, J.A., Cresce, A.V., Ervin, M.H., and Xu, K. (2014). Dual-graphite chemistry enabled by a high voltage electrolyte. *Energy Environ. Sci.* 7, 617–620.

66. Xu, J., Dou, Y., Wei, Z., Ma, J., Deng, Y., Li, Y., Liu, H., and Dou, S. (2017). Recent progress in graphite intercalation compounds for rechargeable metal (Li, Na, K, Al)-ion batteries. *Adv. Sci.* 4, 1700146.

67. Sole, C., Drewett, N.E., and Hardwick, L.J. (2014). *In situ* Raman study of lithium-ion intercalation into microcrystalline graphite. *Faraday Discuss* 172, 223–237.

68. Tobias, P., Sergej, R., Olga, F., Paul, M., Simon Franz, L., Jessica, H., Hinrich-Wilhelm, M., and Martin, W. (2013). Influence of graphite characteristics on the electrochemical intercalation of bis(trifluoromethanesulfonyl) imide anions into a graphite-based cathode. *J. Electrochem. Soc.* 160, A1719–A1991.

69. Qin, P., Wang, M., Li, N., Zhu, H., Ding, X., and Tang, Y. (2017). Bubble-sheet-like interface design with an ultrastable solid electrolyte layer for high-performance dual-ion batteries. *Adv. Mater.* 29, 1606805.

70. Li, W.H., Ning, Q.L., Xi, X.T., Hou, B.H., Guo, J.Z., Yang, Y., Chen, B., and Wu, X.L. (2019). Highly improved cycling stability of anion de-intercalation in the graphite cathode for dual-ion batteries. *Adv. Mater.* 31, e1804766.

71. Jiang, C., Xiang, L., Miao, S., Shi, L., Xie, D., Yan, J., Zheng, Z., Zhang, X., and Tang, Y. (2020). Flexible interface design for stress regulation of a silicon anode toward highly stable dual-ion batteries. *Adv. Mater.* 32, e1908470.

72. Zhang, X., Tang, Y., Zhang, F., and Lee, C. (2016). A novel aluminum-graphite dual-ion battery. *Adv. Energy Mater.* 6, 1502588.

73. Sheng, M., Zhang, F., Ji, B., Tong, X., and Tang, Y. (2017). A novel tin-graphite dual-ion battery based on sodium-ion electrolyte with high energy density. *Adv. Energy Mater.* 7, 1601963.

74. Kravchyk, K.V., Bhauriyal, P., Piveteau, L., Guntlin, C.P., Pathak, B., and Kovalenko, M.V. (2018). High-energy-density dual-ion battery for stationary storage of electricity using concentrated potassium fluorosulfonylimide. *Nat. Commun.* 9, 4469.

75. Wang, G., Kohn, B., Scheler, U., Wang, F., Oswald, S., Löffler, M., Tan, D., Zhang, P., Zhang, J., and Feng, X. (2020). A high-voltage, dendrite-free, and durable Zn-graphite battery. *Adv. Mater.* 32, e1905681.

76. Wang, M., Jiang, C., Zhang, S., Song, X., Tang, Y., and Cheng, H.M. (2018). Reversible calcium alloying enables a practical room-temperature rechargeable calcium-ion battery with a high discharge voltage. *Nat. Chem.* 10, 667–672.

77. Ji, B., Zhang, F., Song, X., and Tang, Y. (2017). A novel potassium-ion-based dual-ion battery. *Adv. Mater.* 29, 1700519.

78. Chen, Z., Tang, Y., Du, X., Chen, B., Lu, G., Han, X., Zhang, Y., Yang, W., Han, P., Zhao, J., and Cui, G. (2020). Anion solvation reconfiguration enables high-voltage carbonate electrolytes for stable Zn/graphite cells. *Angew. Chem. Int. Ed. Engl.* 59, 21769–21777.

79. Xie, D., Zhang, M., Wu, Y., Xiang, L., and Tang, Y. (2020). A flexible dual-ion battery based on sodium-ion quasi-solid-state electrolyte with long cycling life. *Adv. Funct. Mater.* 30, 1906770.

80. Chen, G., Zhang, F., Zhou, Z., Li, J., and Tang, Y. (2018). A flexible dual-ion battery based on PVDF-HFP-modified gel polymer electrolyte with excellent cycling performance and superior rate capability. *Adv. Energy Mater.* 8, 1801219.

81. Li, Z., Liu, J., Niu, B., Li, J., and Kang, F. (2018). A novel graphite-graphite dual ion battery using an $\text{AlCl}_3\text{-}[\text{EMIm}]\text{Cl}$ liquid electrolyte. *Small* 14, e1800745.

82. Beltrop, K., Beuker, S., Heckmann, A., Winter, M., and Placke, T. (2017). Alternative electrochemical energy storage: potassium-based dual-graphite batteries. *Energy Environ. Sci.* 10, 2090–2094.

83. Kravchyk, K.V., Seno, C., and Kovalenko, M.V. (2020). Limitations of chloroaluminate ionic liquid anolytes for aluminum-graphite dual-ion batteries. *ACS Energy Lett.* 5, 545–549.

84. Shi, X., Zhang, W., Wang, J., Zheng, W., Huang, K., Zhang, H., Feng, S., and Chen, H. (2016). $(\text{EMIm})^+(\text{PF}_6^-)$ ionic liquid unlocks optimum energy/power density for architecture of nanocarbon-based dual-ion battery. *Adv. Energy Mater.* 6, 1601378.

85. Elia, G.A., Greco, G., Kamm, P.H., García-Moreno, F., Raoux, S., and Hahn, R. (2020). Simultaneous X-ray diffraction and tomography operando investigation of aluminum/graphite batteries. *Adv. Funct. Mater.* 30, 2003913.

86. Jouhara, A., Quarez, E., Dolhem, F., Armand, M., Dupré, N., and Poizot, P. (2019). Tuning the chemistry of organonitrogen compounds for promoting all-organic anionic rechargeable batteries. *Angew. Chem. Int. Ed. Engl.* 58, 15680–15684.

87. Li, Q., Qiao, Y., Guo, S., Jiang, K., Li, Q., Wu, J., and Zhou, H. (2018). Both cationic and anionic Co (de)intercalation into a metal-oxide material. *Joule* 2, 1134–1145.

88. Aubrey, M.L., and Long, J.R. (2015). A dual-ion battery cathode via oxidative insertion of anions in a metal-organic framework. *J. Am. Chem. Soc.* 137, 13594–13602.

89. Wang, H.G., Wang, H., Si, Z., Li, Q., Wu, Q., Shao, Q., Wu, L., Liu, Y., Wang, Y., Song, S., and Zhang, H. (2019). A bipolar and self-polymerized phthalocyanine complex for fast and tunable energy storage in dual-ion batteries. *Angew. Chem. Int. Ed. Engl.* 58, 10204–10208.

90. Rodríguez-Pérez, I.A., Jian, Z., Waldenmaier, P.K., Palmisano, J.W., Chandrabose, R.S., Wang, X., Lerner, M.M., Carter, R.G., and Ji, X. (2016). A hydrocarbon cathode for dual-ion batteries. *ACS Energy Lett.* 1, 719–723.

91. Rodríguez-Pérez, I.A., and Ji, X. (2017). Anion hosting cathodes in dual-ion batteries. *ACS Energy Lett.* 2, 1762–1770.

92. Fan, L., Liu, Q., Xu, Z., and Lu, B. (2017). An organic cathode for potassium dual-ion full battery. *ACS Energy Lett.* 2, 1614–1620.

93. Zhao, R., Liang, Z., Zou, R., and Xu, Q. (2018). Metal-organic frameworks for batteries. *Joule* 2, 2235–2259.

94. Zhang, Y., An, Y., Yin, B., Jiang, J., Dong, S., Dou, H., and Zhang, X. (2019). A novel aqueous ammonium dual-ion battery based on organic polymers. *J. Mater. Chem. A* 7, 11314–11320.

95. Wrogemann, J.M., Künne, S., Heckmann, A., Rodríguez-Pérez, I.A., Siozios, V., Yan, B., Li, J., Winter, M., Beltrop, K., and Placke, T. (2020). Development of safe and sustainable dual-ion batteries through hybrid aqueous/nonaqueous electrolytes. *Adv. Energy Mater.* 10, 1902709, <https://doi.org/10.1002/aenm.201902709>.

96. Tao, Y., Ding, C., Tan, D., Yu, F., and Wang, F. (2018). Aqueous dual-ion battery based on a hematite anode with exposed {104} facets. *ChemSusChem* 11, 4269–4274.

97. Guo, Q., Kim, K., Jiang, H., Zhang, L., Zhang, C., Yu, D., Ni, Q., Chang, X., Chen, T., Xia, H., and Ji, X. (2020). A high-potential anion-insertion carbon cathode for aqueous zinc dual-ion battery. *Adv. Funct. Mater.* 30, 2002825.

98. Gao, L., Li, Z., Zou, Y., Yin, S., Peng, P., Shao, Y., and Liang, X. (2020). A high-performance aqueous zinc-bromine static battery. *iScience* 23, 101348–101374.

99. Liu, H., Chen, C.Y., Yang, H., Wang, Y., Zou, L., Wei, Y.S., Jiang, J., Guo, J., Shi, W., Xu, Q., and Cheng, P. (2020). A zinc-dual-halogen battery with a molten hydrate electrolyte. *Adv. Mater.* 32, e2004553.

100. Zhang, Z.S., Hu, X.Q., Zhou, Y., Wang, S.F., Yao, L.M., Pan, H., Su, C.Y., Chen, F.M., and Hou, X.H. (2018). Aqueous rechargeable dual-ion battery based on fluoride ion and sodium ion electrochemistry. *J. Mater. Chem. A* 6, 8244–8250.